




N4BP1 mediates RAM domain-dependent notch signaling turnover during neocortical development

Zhihua Ma^{1,†}, Yi Zeng^{1,†,‡} , Ming Wang^{1,†,§}, Wei Liu¹, Jiafeng Zhou¹, Chao Wu¹, Lin Hou^{1,2}, Bin Yin^{1,2}, Boqin Qiang^{1,2}, Pengcheng Shu^{1,2,3,*}  & Xiaozhong Peng^{1,4,5,*} 

Abstract

Notch signaling pathway activity, particularly fluctuations in the biologically active effector fragment NICD, is required for rapid and efficient dynamic regulation of proper fate decisions in stem cells. In this study, we identified NEDD4-binding protein 1 (N4BP1), which is highly expressed in the developing mouse cerebral cortex, as a negative modulator of Notch signaling dynamics in neural progenitor cells. Intriguingly, N4BP1 regulated NICD stability specifically after Notch1 S3 cleavage through ubiquitin-mediated degradation that depended on its RAM domain, not its PEST domain, as had been extensively and previously described. The CoCUN domain in N4BP1, particularly the “Phe-Pro” motif (862/863 amino acid), was indispensable for mediating NICD degradation. The Ring family E3 ligase Trim21 was, in contrast to other NEDD4 family members, required for N4BP1-regulated NICD degradation. Overexpression of N4BP1 in cortical neural progenitors promoted neural stem cell differentiation, whereas neural progenitor cells lacking N4BP1 were sensitized to Notch signaling, resulting in the maintenance of stem-like properties in neural progenitor cells and lower production of cortical neurons.

Keywords N4BP1; neocortical development; Notch signaling; RAM domain; Trim21

Subject Categories Development; Neuroscience; Signal Transduction

DOI 10.15252/embj.2022113383 | Received 24 December 2022 | Revised 6 September 2023 | Accepted 7 September 2023 | Published online 9 October 2023

The EMBO Journal (2023) 42: e113383

Introduction

Notch signaling is an evolutionarily conserved pathway that plays a crucial role in the execution of cell fate determination in a wide

variety of lineages (Artavanis-Tsakonas *et al.*, 1999; Yoon & Gaiano, 2005; Andersson *et al.*, 2011). One of the best examples of Notch signaling is found in the nervous system, where Notch is known to influence the asymmetric cell division of neuroblasts in the *Drosophila* nervous system (Artavanis-Tsakonas *et al.*, 1991; Louvi & Artavanis-Tsakonas, 2006). In the developing mammalian neocortex, Notch signaling is thought to maintain the self-renewal of neural progenitor cells (NPCs), also known as radial glial cells (RGCs), while inhibiting neuronal differentiation, thus maintaining a progenitor pool (Mizutani & Saito, 2005; Mizutani *et al.*, 2007; Kageyama *et al.*, 2009; Aguirre *et al.*, 2010). Hence, accurate and dynamic regulation of Notch signaling is fundamental for brain development, which is controlled by the proper balance between the self-renewal of progenitors and the differentiation of progeny cells.

To generate a variety of physiological outcomes in different cellular contexts, it is necessary to generate the proper Notch signaling activity at the right time and place. Hyperactivation or loss of Notch function results in a wide range of human disorders (Masek & Andersson, 2017). In stark contrast to most signaling pathways, the Notch signaling pathway is not amplified by secondary messenger cascades (Bray, 2006). Moreover, it is activated through the proteolysis of Notch receptors, which releases the active Notch intracellular domain (NICD). The NICD domain is subsequently translocated into the nucleus where it forms a transcriptional activation complex with the DNA-binding protein CSL (*CBF1*, *Su(H)*, or *LAG-1*, also called *RBPJ*) and the coactivator Mastermind (*MAML1*) to promote the transcription of target genes, such as *Hes*, *Hey*, and *BLBP* (Schroeter *et al.*, 1998; Kageyama & Ohtsuka, 1999; Anthony *et al.*, 2005; Borggreffe & Oswald, 2009). A large number of factors have been proven to participate in core Notch pathway regulation, among which the posttranslational modification of NICD is particularly important because Notch signaling activity is largely determined by the level or status of NICD (Schroeter *et al.*, 1998; Fortini, 2009; Bray, 2016).

1 Department of Molecular Biology and Biochemistry, Medical Primate Research Center, Neuroscience Center, Institute of Basic Medical Sciences, Chinese Academy of Medical Sciences, School of Basic Medicine Peking Union Medical College, Beijing, China

2 State Key Laboratory of Common Mechanism Research for Major Diseases, Beijing, China

3 Chinese Institute for Brain Research, Beijing, China

4 State Key Laboratory of Respiratory Health and Multimorbidity, Beijing, China

5 Institute of Laboratory Animal Science, Chinese Academy of Medical Sciences, Peking Union Medical College, Beijing, China

*Corresponding author. Tel: +86 10 69156434; E-mail: pengcheng_shu@ibms.pumc.edu.cn

**Corresponding author. Tel: +86 10 65105087; E-mail: pengxiaozhong@pumc.edu.cn

†These authors contributed equally to this work

‡Present address: Department of Infectious Diseases, Institute for Viral Hepatitis, The Key Laboratory of Molecular Biology for Infectious Diseases (Ministry of Education), The Second Affiliated Hospital of Chongqing Medical University, Chongqing, China

§Present address: Department of Otolaryngology, Head and Neck Surgery, Beijing Tongren Hospital, Capital Medical University, Beijing Key Laboratory of Nasal Diseases, Beijing Institute of Otolaryngology, Beijing, China

Various posttranslational modifications, including ubiquitination, phosphorylation, acetylation, and hydroxylation, of NICD have been shown to regulate pathway signaling (Fortini, 2009; Andersson et al, 2011). For instance, Sirt1 interacts with NICD and acts as a deacetylase that attenuates acetylation-induced NICD stabilization (Guarani et al, 2011).

Experiments on the ubiquitination of NICD have shed light on the regulation of the NICD half-life, and several E3 ligases and deubiquitinating enzymes have been identified; among these proteins, the HECT (homologous to the E6AP carboxyl terminus) family of E3 ligases, including Nedd4 and Itch (Su(dx) in flies), and the RING (really interesting new gene) family E3 ligases Deltex (Dutta et al, 2022), Itch and Nedd4 have been shown to be involved in the endocytic trafficking of Notch (Qiu et al, 2000; Lai, 2002). Previously, the most important E3 ligase shown to influence the stability of NICD in mammals was Fbw-7 (F-box and WD repeat domain-containing 7 and its orthologues SEL-10 in *Caenorhabditis elegans* and Archipelago in flies), which ubiquitinated the NICD sequence within the NICD PEST (rich in proline, glutamic acid, serine, and threonine residues) domain in the nucleus, leading to the degradation of NICD (Oberge et al, 2001; Wu et al, 2001; Fryer et al, 2004). Disruption of Fbw7 in the mouse brain severely impaired stem cell differentiation and increased progenitor cell death via the upregulation of NICD and the phosphorylation of c-Jun (Hoeck et al, 2010). However, whether degradation mechanisms in addition to PEST are involved in Notch signaling remains to be determined. For example, Shaye and Greenwald found that the RAM (RBPjk association module) domain in NICD mediated Notch degradation in *C. elegans* (Shaye & Greenwald, 2002), but whether this mechanism is conserved in mammals is unclear, and the molecules that are involved in this regulatory effect have not been elucidated.

In this study, we identified an NICD turnover mechanism that does not involve the PEST domain and identified N4BP1 (NEDD4 binding protein 1) as an antagonist of Notch signaling that exerts its effect by regulating the stabilization of NICD during neurogenesis. N4BP1 was first identified as a monoubiquitination substrate of the E3 ligase Nedd4 (Murillas et al, 2002) and later was shown to interact with

another E3 ligase, Itch, which protected p73 α /HER3 from Itch-induced degradation (Oberst et al, 2007). Michael R. Kuehn et al found that N4BP1 was mainly located in the nucleolus and underwent SUMOylation and ubiquitylation, regulating its turnover (Sharma et al, 2010). N4BP1 has been reported to carry an RNA-binding K homology (KH) domain, a potential RNA nuclease (RNase) domain (NYN domain), and two putative ubiquitin chain-binding domains (Anantharaman & Aravind, 2006; Gitlin et al, 2020). In this study, we identified the C-terminal ubiquitin-binding domain of N4BP1, named the CoCUN domain, involved in the polyubiquitination of NICD via a conserved N4BP1 Phe-pro motif (Nepravishta et al, 2019)[‡]. These findings underscore N4BP1 as a novel endogenous regulator of the Notch signaling pathway, which is involved in maintaining the precise balance between the proliferation and differentiation of NPCs.

Results

N4BP1 antagonizes notch activity by mediating NICD degradation

As measured by immunoblotting, N4BP1 was found to be expressed in various tissues of adult mice and to be particularly enriched in the brain. Specifically, N4BP1 was abundantly expressed in the telencephalon and thalamus in adult mouse brain tissue (Fig EV1A and B). In the developing mouse brain, *n4bp1* mRNA was mainly expressed in the ventricular zone (VZ) after embryonic day (E) 12.5 through postnatal day (P) 3, as measured via *in situ* hybridization (ISH). Notably, the expression of *n4bp1* mRNA increased significantly between E12.5 and E14.5, which was consistent with the transition of RGCs from being a predominantly proliferation state to the onset of differentiation, suggesting a potential role for N4BP1 in the differentiation of neural stem cells (Fig EV1C).

To assess the function of N4BP1, *in utero* electroporation (IUE) was performed to transiently overexpress N4BP1 in RGCs on E13.5 (Fig EV2A). The ectopic expression of N4BP1 was notable at E15.5 (Fig EV2B and C). When harvested on E16.5, compared with the

Figure 1. N4BP1 inhibits the Notch signaling pathway *in vivo* and *in vitro*.

- A Sections of E16.5 brains carrying control, N4BP1, DN-MAML, NICD, and N4BP1 plus NICD plasmids. White-dotted rectangles mark comparable regions of the cortex shown below at higher magnification after staining for the apical progenitor marker Sox2. The white dotted lines display the boundary between VZ and SVZ regions. Scale bars represent 200 and 50 μ m for up and down panels respectively.
- B, C Quantitative analysis of GFP⁺ cell distribution in neocortex divided into six bins (B) and GFP⁺ cells coexpressed various markers (C) ($n = 5$ for control group, $n = 4$ for N4BP1 group, $n = 3$ for NICD group and $n = 4$ for N4BP1 + NICD group). The deep blue star: N4BP1 versus control; the green star: N4BP1 + NICD versus NICD.
- D Measurements of wtCBF-1 luciferase activity after transfection with control, DN-MAML or N4BP1; mock was an empty control. $n = 4$ biological replicates.
- E qPCR measurements of the Notch pathway target genes *Hey1* and *BLBP* after co-transfection with the control or N4BP1 plus NICD plasmid. $n = 3$ biological replicates.
- F, G Western blot detection of NICD protein after different doses (250 and 500 ng) of N4BP1 overexpression in HEK293T cells (F) or knocked down of N4BP1 in N1E-115 cells (G). pCIG is used as the control vector for the N4BP1 plasmid.
- H Measurements of wtCBF-1 luciferase activity after co-transfection of N4BP1 shRNA with NICD in N1E-115 cells. $n = 3$ biological replicates.
- I Representative sections of brains electroporated with N4BP1-G and low (L) or high (H) dose of NICD-R plasmid. White-dotted rectangles mark comparable regions of the cortex shown below at 40 \times higher magnification, and the white-dotted circles represent red fluorescence in NICD-R transfected cells. $n = 3$ for each group. Scale bars represent 200 and 50 μ m for up and down panel respectively.
- J Quantification of the red fluorescence intensity emitted by NICD-mCherry. $n = 4$ for NICD-R (L) group, and $n = 3$ for other groups, biological replicates.
- Data information: The mean \pm SD. is shown. Statistical analysis was performed by unpaired two-tailed Student's *t* test; * $P < 0.05$; ** $P < 0.01$; and *** $P < 0.001$. Source data are available online for this figure.

[‡]Correction added on 15 November 2023, after first online publication: The sentence has been corrected from "...polyubiquitination of NICD via a conserved NICD Phe-pro motif..." to "...polyubiquitination of NICD via a conserved N4BP1 Phe-pro motif".

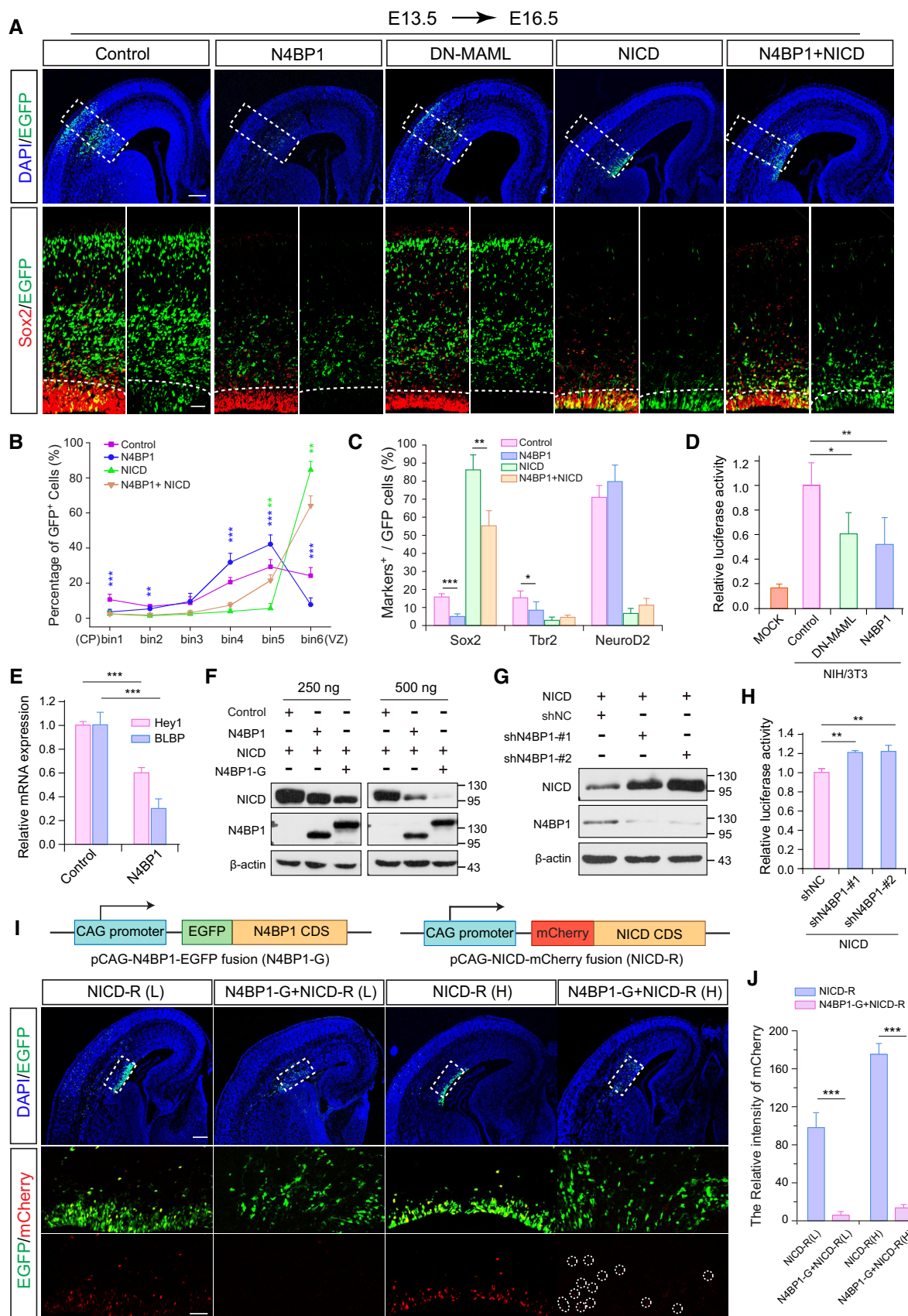


Figure 1.

control group, GFP⁺ cells that overexpressed N4BP1 were relatively scarce in the germinal zone (VZ and subventricular zone (SVZ)) and cortical plate (CP), as they were largely restricted to the intermediate zone (IZ). When dividing the cerebral cortex into six equal parts (bin1–bin6), GFP⁺ cells were found to be distributed as follows: 24.16 ± 4.71% in bin 6 of the control group versus 7.69 ± 3.87% in the N4BP1 group, and 29.29 ± 4.11% versus 42.14 ± 5.34% in bin 5 (Figs 1A and B, and EV2D and E). Moreover, the ratio of GFP⁺ cells colabeled with Sox2 (an RGC marker) was decreased, from 15.81 ± 1.81% in the control group to 5.02 ± 1.45% in the N4BP1 group. GFP⁺ cells colabeled Tbr2 (an intermediate progenitor marker) declined from 15.34 ± 3.78% in the control group to 8.47 ± 4.62% in the N4BP1 group (Figs 1C, and EV2D and F). These data imply that overexpression of N4BP1 promotes neurogenesis *in vivo*.

As the Notch signaling pathway is necessary for the stemness maintenance of RGCs, NICD, and DN-MAML plasmids were used to mimic and inhibit the activity of Notch signaling, respectively. IUE was performed at E13.5 and harvested at E16.5. The results showed that different doses of NICD overexpression plasmids revealed the dose-dependent activation of Notch signaling (Appendix Fig S1). GFP⁺ cells were mainly localized to the VZ and showed Sox2-positive NPC characteristics (Fig EV3A and Appendix Fig S1). In contrast, the DN-MAML plasmid drove all GFP⁺ cells out of the VZ, inducing their differentiation into neurons, in contrast to its effect on the control group cells (Fig 1A). When N4BP1 and NICD were simultaneously overexpressed after coelectroporation with the N4BP1 and NICD plasmids, fewer GFP⁺ cells remained in the VZ, and more GFP⁺ cells were found in the intermediate zone, in contrast to the distribution of these cells in the NICD group (Figs 1A and EV3A). Both the N4BP1 plasmid and N4BP1-GFP fusion plasmid (N4BP1-G) induced a similar dose-dependent antagonizing effect on NICD. A significant proportion of GFP⁺ cells translocated from the VZ and to the IZ. The distribution of GFP⁺ cells was increased in bin 5 (21.42 ± 4.08% (N4BP1 + NICD group) versus 5.54 ± 2.88% (NICD group)) at the expense of the number of cells in bin 6 (64.09 ± 6.25% (N4BP1 + NICD group) versus 84.5 ± 4.86% (NICD group); Fig 1B). Moreover, in the N4BP1 + NICD group, the percentage of GFP⁺ cells coexpressed with Sox2 declined to 55.28 ± 8.32%, compared with the NICD group (86.24 ± 8.32%; Fig 1C).

Additionally, a canonical coculture system was used to further investigate the antagonizing effect of N4BP1 on endogenous Notch signaling. A luciferase construct containing four CBF1-binding sites (4 × CBF1-Luc) was transiently transfected into C2C12 myoblast cells that express endogenous Notch. C2C12 cells were then cocultured with ligand-expressing NIH/3T3 cells to activate endogenous Notch signaling. Luciferase activity was significantly decreased when DN-MAMAL or N4BP1 was overexpressed in C2C12 cells (Fig 1D). Similarly, when cotransfection of N4BP1 with NICD plasmid, the expression of Notch pathway target genes, such as Hey1 and BLBP, is obviously downregulated (Fig 1E). Additionally, NICD was co-transfected with different doses of N4BP1 in HEK293T cells which is absent for N4BP1 expression. The protein expression of NICD was found to be significantly downregulated in an N4BP1 dose-dependent manner (Fig 1F). In contrast, when the knockdown of N4BP1 in N1E-115 cells, the protein levels of NICD and Notch pathway activity increased notably (Fig 1G and H).

To investigate whether N4BP1 accelerates the degradation of NICD *in vivo*, the N4BP1-EGFP fusion plasmid (N4BP1-G) and

NICD-mCherry fusion plasmid (NICD-R) were co-electroporated into the mouse brain on E13.5 and harvested on E14.5 and E16.5. Similar to the results *in vitro*, N4BP1 overexpression drove GFP⁺ cells away from the apical surface of the VZ, and mediated NICD degradation in a dose-dependent manner. The mCherry fluorescence intensity was significantly weaker in the N4BP1 group than in the control group (Figs 1I and J, and EV3B). To exclude the possible influence of N4BP1 on the transcriptional activity of the NICD vector, the control vector pCAG-mCherry was co-electroporated with N4BP1 plasmid by IUE. The results showed that the intensity of mCherry was not affected by N4BP1 overexpression (Fig EV3C). Similarly, cotransfection of N4BP1 with other overexpression constructs also excluded the possible influence on the transcriptional activity of pCAG vectors (Fig EV3D). Overall, N4BP1 promotes neurogenesis by mediating NICD degradation.

N4BP1 promotes NICD protein turnover through the ubiquitin–proteasome pathway

To dissect the mechanism of N4BP1-mediated negative regulation of NICD, coimmunoprecipitation (co-IP) was carried out after the transfection of the N4BP1 plasmid into N1E-115 cells. Liquid chromatography–tandem mass spectrometry analysis (LC–MS/MS) was performed, and NICD was identified as an N4BP1-interacting protein (Fig 2A). When His-N4BP1 was co-transfected with Flag-NICD into HEK293T cells, N4BP1 was detected via immunoprecipitation with an anti-Flag antibody, and alternatively, NICD was detected after immunoprecipitation with an anti-His antibody (Fig 2B), which indicated the direct interaction between N4BP1 and NICD at the protein level. Furthermore, HEK293T cells were cotransfected with N4BP1 and NICD, and treated with cycloheximide to evaluate the effects of N4BP1 on NICD protein stability. Compared to that in the control group, NICD protein expression was attenuated more quickly in the N4BP1-overexpression group (Fig 2C). In contrast, knocking down N4BP1 by shN4BP1-1# and 2# both stabilized the NICD protein (Figs 2D and EV3E).

To investigate whether the full-length Notch1 (Notch1-fl) was regulated by N4BP1 overexpression, C2C12 cells were transfected with N4BP1 plasmid and cocultured with ligand-expressing NIH/3T3 cells. Intriguingly, although NICD was significantly decreased, both the endogenous Notch1-fl and Notch1 transmembrane and intracellular domain (TM-NICD) were not affected by N4BP1 overexpression (Fig 2E). To further confirm this finding, N4BP1, and Notch1-fl plasmid were then co-transfected in HEK293T cells, and the membrane protein was isolated and analyzed for the surface expression of Notch1. The results showed that membrane Notch1 (Notch1-fl and TM-NICD) was not influenced by N4BP1 overexpression (Fig 2F). These findings indicated that N4BP1 regulated NICD stability specifically after Notch1 S3 cleavage.

To confirm the pathway through which N4BP1 mediated NICD degradation, MG132 and chloroquine were used to block the ubiquitin–proteasome system and lysosomal proteolysis pathway, respectively. MG132 treatment inhibited N4BP1-mediated NICD degradation, while chloroquine did not alter N4BP1-mediated degradation of the NICD protein (Fig 2G). In addition, co-expression of HA-Ub with NICD led to the formation of a high-molecular-weight smear after anti-Flag immunoprecipitation. Co-transfection of N4BP1 with NICD in HEK293T cells led to markedly rapid Notch-Ub conjugation,

which was further accelerated by MG132 treatment (Fig 2H). These data indicated that N4BP1 forced ubiquitin-dependent proteasomal degradation of NICD, thereby reducing Notch pathway activity.

As previous studies have shown that N4BP1 was predominantly located in the nucleolus (Sharma et al, 2010; Gou et al, 2021), we evaluated the distribution of N4BP1 in the nucleus and cytoplasm. In the E14.5 brain, E18.5 dorsal telencephalon, cultured NPCs, and N1E-115 cells, N4BP1 was distributed mainly in the cytoplasm, and few in the nucleus. Knocking down N4BP1 in N1E-115 cells efficiently downregulated cytoplasmic and nuclear N4BP1 (Appendix Fig S2A). Transfection of N4BP1-G plasmid into N1E-115 cells, the exogenous

expression of N4BP1 (fused with EGFP) was found to be distributed mainly in the cytoplasm with few molecules in the nucleus, shown as puncta (Appendix Fig S2B). The subcellular distribution of N4BP1 indicates that it can possibly regulate NICD via proteolysis.

The RAM domain is necessary for N4BP1-mediated NICD degradation

The well-characterized ubiquitin-proteasome pathway of NICD degradation relies on the PEST domain (Bray, 2016). To evaluate whether N4BP1-mediated NICD degradation also depends on the

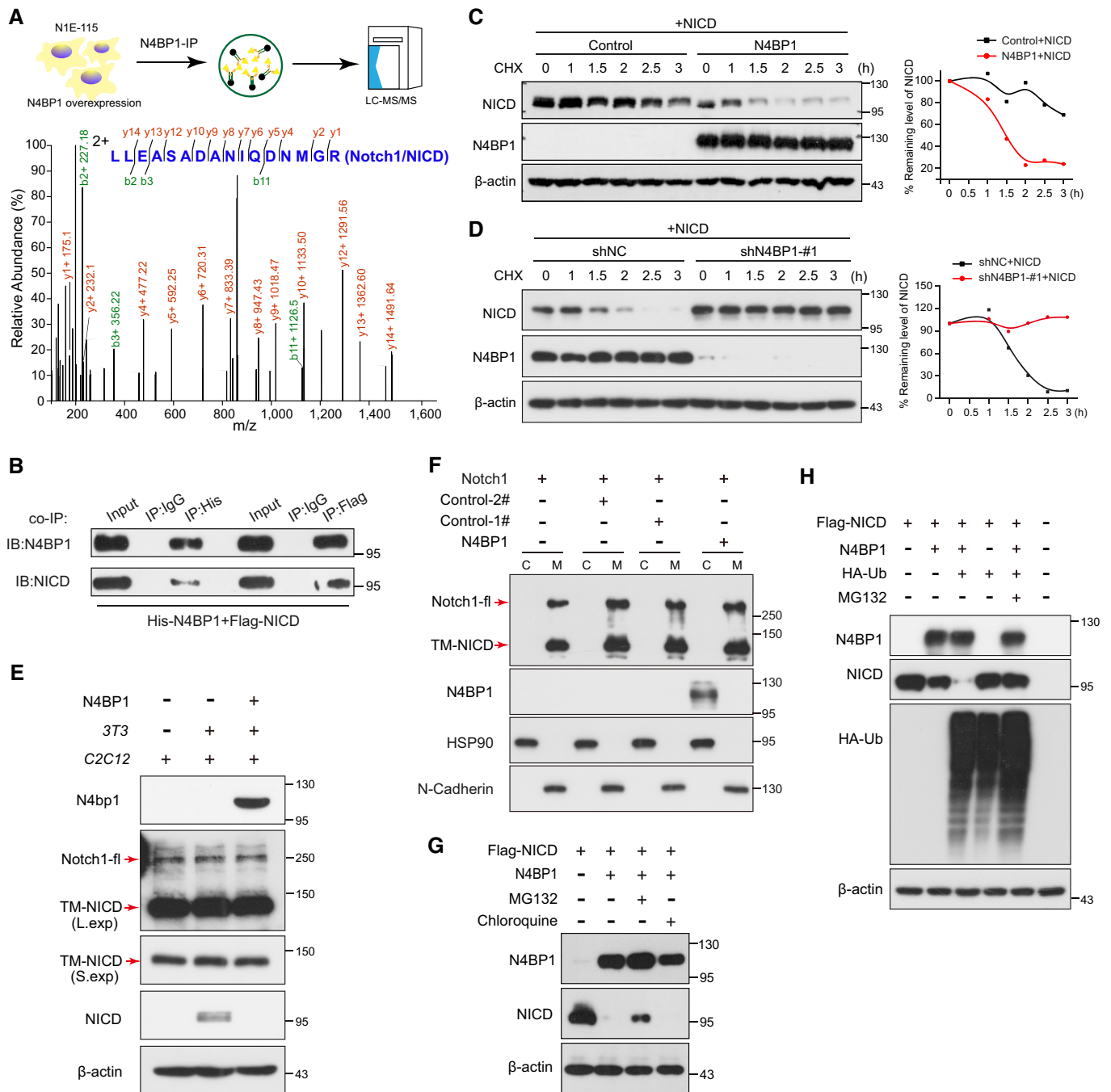


Figure 2.

Figure 2. N4BP1 mediates NICD protein turnover directly through the ubiquitin–proteasome pathway.

- A LC–MS/MS spectrum verification of N4BP1 immunoprecipitates in N1E-115 cells. The general workflow of co-IP combined with LC–MS/MS assays.
- B Immunoblots showing immunoprecipitates obtained with anti-Flag antibody and anti-His antibody after Flag-NICD and His-N4BP1 co-transfection, respectively. IP, immunoprecipitation; IB, immunoblot.
- C, D NICD protein levels analyzed at the indicated time points after cycloheximide (CHX, 50 $\mu\text{g}/\text{ml}$) treatment and co-transfection NICD with N4BP1 in HEK293T cells (C) or shN4BP1 in N1E-115 cells (D).
- E Influence of N4BP1 on endogenous Notch1-fl, TM-NICD, and NICD. C2C12 cells were transfected with N4BP1 plasmid and cocultured with NIH/3T3 cells. The expression levels of Notch1-fl, TM-NICD, and NICD were determined by immunoblot.
- F Influence of N4BP1 on surface expression of Notch1. N4BP1 and Notch1-fl plasmid were co-transfected in HEK293T cells, and the membrane protein was isolated and analyzed. pCIG and pCAG vectors were used as Control #1 and Control #2 respectively.
- G NICD protein expression in HEK293T cells treated with chloroquine (20 μM) or MG132 (10 μM) for 6 h after transfection with NICD with/without N4BP1 for 30 h.
- H Immunoblots show the ubiquitinated NICD levels. Anti-HA antibody and anti-Flag antibody were used to show the Ub and NICD in cells treated with/without MG132 (10 μM) for 6 h after transfection with NICD with/without N4BP1 or with/without HA-Ub for 30 h. pCIG is used as the control to adjust the amount for transfection.

Source data are available online for this figure.

PEST domain, a plasmid of NICD mutant lacking the PEST domain (NICD Δ PEST) was constructed (Fig 3A and Appendix Fig S3A). After transfection, compared with wild-type NICD, the NICD Δ PEST mutant displayed a longer protein expression half-life (Appendix Fig S3B). Surprisingly, when co-transfected with N4BP1 plasmid, the expression of NICD Δ PEST was still decreased (Fig 3B); and conversely, knocking down N4BP1 led to an increase in NICD Δ PEST expression (Fig 3C), which indicated a PEST domain-independent mechanism of NICD degradation. Similar to the wild-type NICD protein, the NICD Δ PEST protein vanished rapidly in the group co-transfected with N4BP1 plasmid after cycloheximide treatment (Fig 3D). In contrast, NICD Δ PEST protein stability was increased after N4BP1 knockdown (Fig 3E).

To identify the domain critical for N4BP1-mediated NICD degradation, we subcloned different NICD sequences (Fig 3A and Appendix Fig S3C). After transfection with N4BP1 and different truncation mutant NICD plasmids, immunoblotting was performed, and the results showed that all the truncated construct products containing the RAM domain were significantly degraded by N4BP1 overexpression, either N4BP1 or N4BP1-G plasmid. However, the expression of the ANK, Δ RAM-ANK, and Δ RAM domains was unaffected by N4BP1 (Fig 3F and Appendix Fig S3D). Thus, the results indicated that the RAM domain may be a bona fide pivotal domain mediating NICD degradation in response to N4BP1.

Furthermore, purified GST-RAM or GST protein was co-incubated with E14.5 brain lysates, and the differentially expressed bands were identified by LC–MS/MS (Fig 3G). The results showed that N4BP1 was identified as a protein that interacted with the RAM domain of NICD (Fig 3H). Moreover, His-N4BP1 and Flag-RAM constructs were co-transfected into HEK293T cells, and immunoprecipitation was performed with anti-His and anti-Flag antibodies, respectively. The results confirmed the interaction between N4BP1 and the RAM domain (Fig 3I). These results showed that N4BP1 accelerated NICD degradation via the RAM domain, not the PEST domain.

The CoCUN domain of N4BP1 is required for the regulation of NICD degradation

To identify the key domain of N4BP1 that regulates NICD degradation, different N4BP1 domains, including the KH domain (aa 57–139), UBA domain (aa 343–385), NYN domain (aa 615–767), and CoCUN domain (aa 845–893), were constructed (Fig 4A). After co-transfection of Flag-NICD with different N4BP1 constructs, only the

constructs carrying the CoCUN domain decreased NICD expression at the protein level (Figs 4B and EV4A). As the “Phe-pro” motif (FP) of the CoCUN domain had been reported to be critical to the ubiquitination activity of N4BP1 (Nepravishta *et al*, 2019), we mutated the FP motif to be a “Pro-ala” (PA) motif (N4BP1 Mut), and found that N4BP1 Mut alleviated NICD protein degradation compared to the degradation observed in the N4BP1-overexpressing group (Fig 4C). The NYN domain of N4BP1, which is conserved between species (Fig EV4B), has been found to show RNase activity (Yamasoba *et al*, 2019). We further investigated whether the NYN domain is also associated with the protein degradation of NICD. Notably, NICD protein expression was not affected by the KHNYN protein that harbors the NYN domain (Fig EV4C). Additionally, in accordance with its regulation of NICD, the CoCUN domain alone suppressed the expression of the NICD RAM domain, while the NYN domain exerted no effect on RAM expression (Fig EV4D).

To confirm the role of the CoCUN domain in regulating Notch signaling, N4BP1, N4BP1 Mut, and N4BP1 Δ CoCUN construct were electroporated into the mouse brain on E13.5. Compared with the control group, N4BP1 promoted an increase in GFP⁺ cell escape from the VZ/SVZ (bin6) and entry into the IZ (bins 4 and 5), where they were retained. However, bin 6 of both the N4BP1 Mut and N4BP1 Δ CoCUN groups were significantly enriched with more GFP⁺ cells than that of the N4BP1 group. Similarly, compared with the N4BP1 group, more GFP⁺ cells co-expressing Sox2 were found in both the N4BP1 Mut and N4BP1 Δ CoCUN groups (Fig 4D–F).

Additionally, truncation or mutant plasmids were constructed based on N4BP1-G, including N4BP1 Mut-EGFP fusion (N4BP1-G Mut) and N4BP1 Δ CoCUN-EGFP fusion plasmid (N4BP1-G Δ CoCUN; Fig 4G). When co-electroporated NICD-R with N4BP1-G plasmid, NICD was degraded at the protein level as indicated by the fluorescence intensity of mCherry (Fig 4H). However, neither the N4BP1-G Mut nor the N4BP1-G Δ CoCUN construct could decrease mCherry intensity. Overall, these findings demonstrated that the CoCUN domain in N4BP1 was pivotal for NICD regulation *in vitro* and *in vivo*.

The E3 ubiquitin ligase Trim21 is critical for N4BP1-mediated NICD degradation

E3 ubiquitin ligases are required for ubiquitin-proteolysis and determine the specificity of proteolysis (Santonicio, 2020). To investigate which E3 ubiquitin ligase responded to N4BP1-mediated NICD

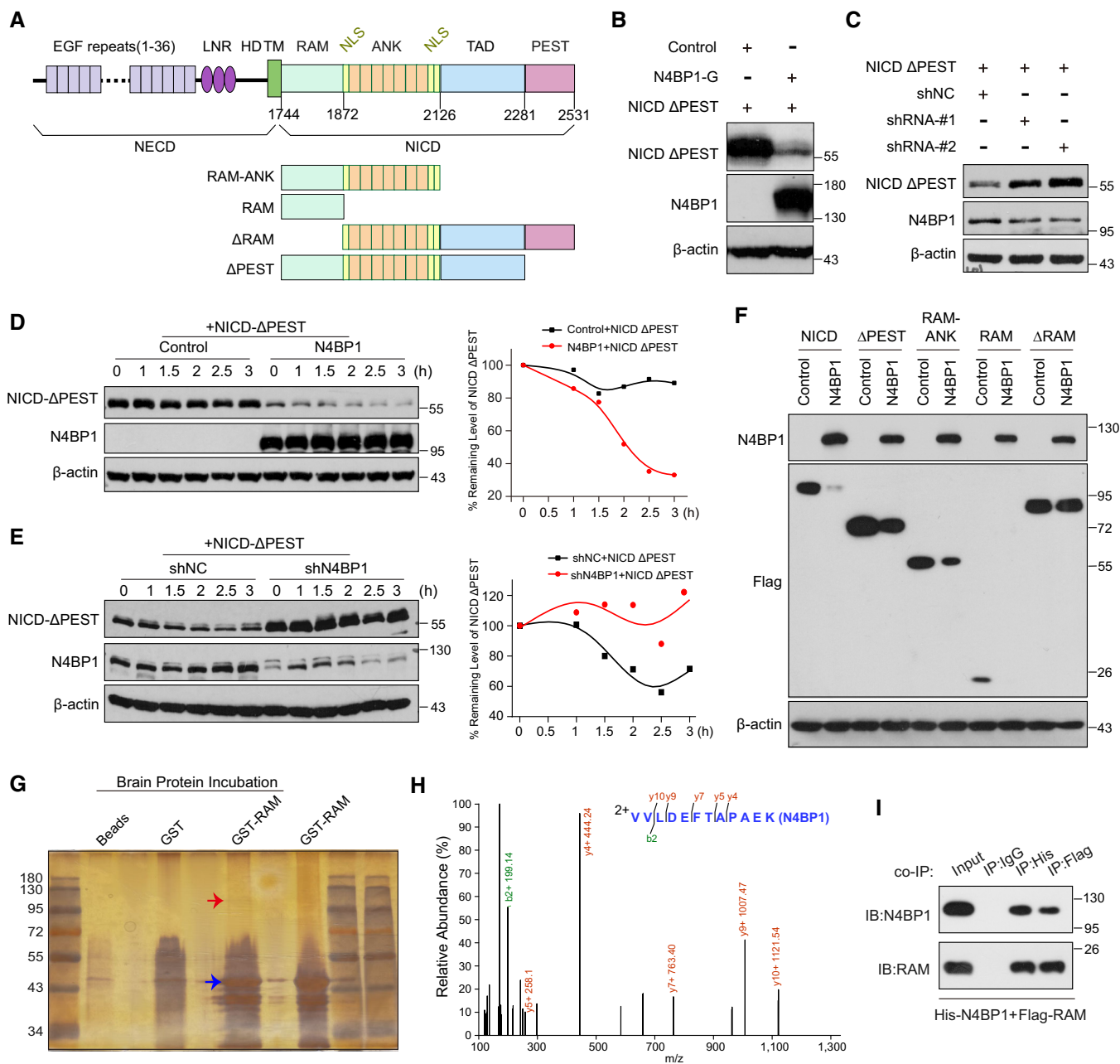


Figure 3. N4BP1 promotes NICD degradation dependent on the RAM domain but not the PEST domain.

A Overview of different NICD domains, including the position details.
 B, C Immunoblot analysis of NICD ΔPEST after co-transfection of NICD ΔPEST with N4BP1 in HEK293T cells (B) or shN4BP1 in N1E-115 cells (C).
 D, E NICD ΔPEST protein levels analyzed at the indicated time points after treatment with cycloheximide (50 μg/ml) and co-transfection of NICD with N4BP1 in HEK293T cells (D) or shN4BP1 in N1E-115 cells (E). The NICD quantitation curve in the right panel was drawn.
 F Influence of N4BP1 co-transfection on the expression of NICD-truncated constructs in HEK293T cells. An anti-Flag antibody was used to detect truncated NICD.
 G, H Silver staining of the GST pull-down protein (G) or LC-MS/MS spectrum verification (H) of GST or GST-RAM incubated with cell lysates of E14.5 brain. The red and blue arrow indicates the potential band of N4BP1 and GST-RAM respectively.
 I Immunoblot measurement of immunoprecipitates with anti-His or anti-Flag antibody after Flag-RAM and His-N4BP1 co-transfection in HEK293T cells.
 Data information: IP, immunoprecipitation; IB, Immunoblot. *n* = 3 independent experiments (unless otherwise specified).
 Source data are available online for this figure.

proteolysis, E3 ligases of the NEDD family which are possibly associated with N4BP1, including NEDD4-1, NEDD4-2, ITCH, SMURF1, SMURF2, WWP1 and WWP2, and the E3 ubiquitin ligase Sel10,

which was reported to promote NICD ubiquitination (Oberg et al, 2001; Wu et al, 2001), were silenced by siRNAs in cells over-expressing N4BP1 and NICD. Surprisingly, none of the above E3

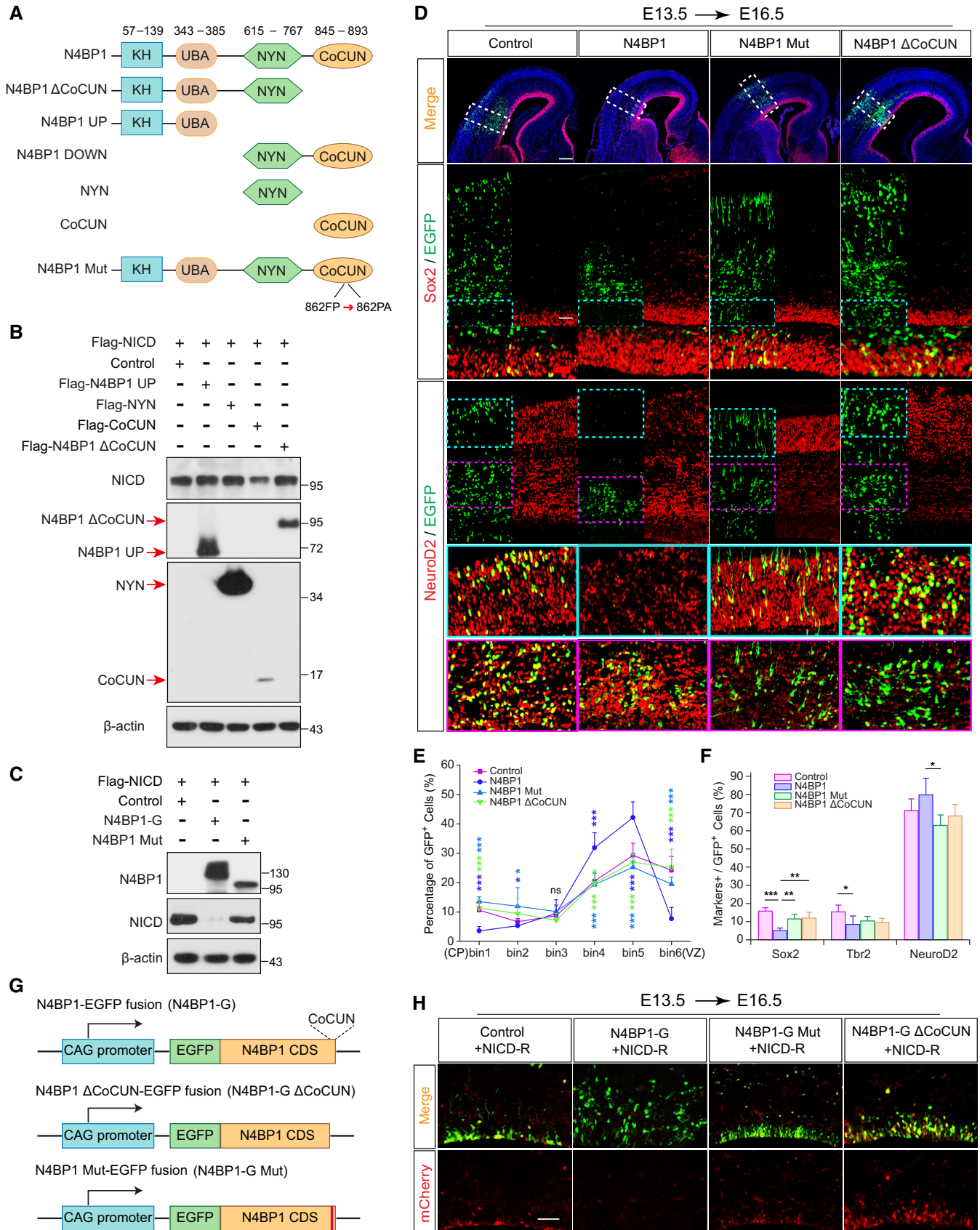


Figure 4.

Figure 4. The CoCUN domain of N4BP1 is critical for the negative regulation of NICD.

- A Overview of N4BP1 subclones with different domains. Details of the amino acid position are included.
- B, C Immunoblot analysis of NICD protein co-transfected with different N4BP1-truncated constructs (B), and N4BP1-G or N4BP1 Mut (C) in HEK293T cells. The red arrows indicate the corresponding truncated N4BP1 bands.
- D Sections of E16.5 brains electroporated on E13.5 with plasmids expressing either control, N4BP1, N4BP1 Mut, or N4BP1 ΔCoCUN. The upper images show the region of IUE; scale bars, 200 μm. White-dotted rectangles mark comparable regions of the cortex shown below at higher magnification; scale bars, 50 μm. The narrow turquoise-dashed boxes show merged images of GFP and Sox2 staining in the VZ are magnified at 2×. The wide turquoise- or pink-dashed boxes are merged images of GFP and NeuroD2 staining in the CP or IZ at the bottom of the respective panels.
- E, F Quantitative analysis of the distribution of GFP⁺ cells after dividing the neocortex into six bins (E) and the fraction coexpressing various markers (Sox2, Tbr2, and NeuroD2) in the transfected neocortices (F) ($n = 5$ for control group, and $n = 4$ for N4BP1, N4BP1 Mut and N4BP1 ΔCoCUN group respectively). The deep blue star: N4BP1 versus control; the light blue star: N4BP1 versus N4BP1 Mut; the green star: N4BP1 versus N4BP1 ΔCoCUN.
- G Schematic diagram of N4BP1, N4BP1 ΔCoCUN, N4BP1 Mut EGFP fusion constructs. The red bold vertical line indicates the amino acid “FP” mutated to “PA”.
- H Representative sections show the NICD expression indicated by the red fluorescence intensity in different groups; scale bars, 50 μm.
- Data information: The mean ± SD is shown. Statistical analyses were performed with one-way ANOVA *post hoc* Bonferroni tests; * $P < 0.05$; ** $P < 0.01$; and *** $P < 0.001$. Source data are available online for this figure.

ubiquitin ligase silencing could attenuate the effect of N4BP1 on NICD degradation (Fig 5A and B).

To further identify the E3 ubiquitin ligase participating in the N4BP1-NICD interaction, N4BP1 co-IP immunoprecipitates of N1E-115 cells were further assessed by LC-MS/MS. In three independent LC-MS/MS assays, a total of 15 E3 ubiquitin ligases were identified, among which only Trim21 was the common molecule (Fig 5C). Co-transfection of N4BP1, NICD, and siRNA targeted Trim21 (siTrim21) was performed, and the result showed that siTrim21 significantly attenuated NICD degradation compared to the siRNA negative control (siNC; Fig 5D). Furthermore, co-transfection of Flag-NICD, N4BP1, HA-Ub, and Trim21 clearly increased NICD ubiquitination, as shown in the anti-HA immunoblot (Fig 5E). Then, we carried out a co-IP assay to confirm that Trim21 directly interacts with NICD. Notably, Flag-NICD and His-Trim21 immunoprecipitated with each other (Fig 5F and G). Co-IP was further performed after co-transfection of N4BP1, His-Trim21, and NICD plasmid. MG132 was added to block the ubiquitin-proteasome degradation of NICD. Co-transfection with N4BP1 significantly increased the NICD level that was immunoprecipitated by the His antibody (Fig 5H), indicating an increased binding ability of Trim21 to NICD. Additionally, Trim21 showed high expression at the protein level in NPCs isolated from the dorsal telencephalon at E14.5 (Fig 5I), indicating the potential interaction between Trim21, NICD, and N4BP1 during the development of the cerebral cortex.

N4BP1 is required for balancing the differentiation and proliferation of RGCs

To further confirm the function of N4BP1 in neural development, conditional N4bp1-knockout (N4bp1-cKO) mice were generated by crossing the N4bp1-Flox mouse strain with Emx1-Cre mice, which resulted in the deletion of exon 2 from N4bp1 (Fig EV5A and B). In the cerebral cortex of E14.5 N4bp1-cKO mice, the expression of N4BP1 protein was depleted, in contrast to WT mice (Fig EV5C). To investigate the effect of N4bp1 ablation during neocortical development, the size of the telencephalon was assessed on P3 by measuring the longitudinal diameter (LD) and transverse diameter (TD; Fig 6A). The LD of the telencephalon from N4BP1-cKO mice ($95.33 \pm 4.95\%$) decreased by approximately 5% compared to WT mice ($100.57 \pm 4.64\%$), while the TD was reduced by approximately 8% ($91.76 \pm 5.54\%$ of N4BP1-cKO mice versus $99.54 \pm 3.64\%$ of WT mice; Fig 6B). In addition, the thickness of the CP was found to be reduced by approximately 15% after N4bp1 ablation (Fig 6C and D).

As the neuronal layer is obviously thinner, we performed immunostaining with specific laminar markers Cux1 (Layers II–IV), Brn2 (mainly layers II–III and V), Ctip2 (Layer V), and Tle4 (Layer VI) to determine the neuronal layers affected by N4bp1 ablation (Figs 6D and EV5D). The immunostaining revealed a major reduction in the number of Cux1⁺ and Brn2⁺ upper-layer neurons; however, the number of Ctip2⁺ and Tle4⁺ neurons were largely unchanged in the N4bp1-cKO mice compared to that in the WT mice (Figs 6E and

Figure 5. Trim21 but not NEDD4 family E3 ubiquitin ligase is involved in N4BP1 mediated NICD degradation.

- A, B Immunoblots showing NICD expression after co-transfection NICD with N4BP1 and siNC or siRNA against NEDD4 E3 ligases NEDD4-1, NEDD4-2, ITCH, SMURF1, SMURF2, WWP1 and WWP2 (A), and Sel10 (B) in N1E-115 cells.
- C The LC-MS/MS spectrum identifies Trim21 in the N4BP1 immunoprecipitates from N1E-115 cells.
- D Immunoblots showing the expression of NICD co-transfected with N4BP1 plasmid and siTrim21 in N1E-115 cells. pCIG is used as the control to adjust the amount for transfection.
- E Western blot measurement of ubiquitinated NICD obtained with an anti-HA antibody in HEK293T cells treated with MG132 (10 mM) for 12 h after cells transfected with NICD plasmid with (+) or without (–) N4BP1, Trim21 and HA-Ub. Cell lysates were incubated with anti-Flag antibody.
- F, G Immunoblots showing protein interactions between Trim21 and NICD. Flag-NICD and His-Trim21 were transfected in HEK293T cells, and co-IP assay was then performed.
- H Co-transfection with N4BP1 significantly increased NICD immunoprecipitated by Trim21. Co-IP was performed using anti-His antibody after co-transfection of N4BP1, His-Trim21, and NICD plasmid in HEK293T cells. pCIG is used as the control to adjust the amount for transfection.
- I Immunoblots showing Trim21 expression in neural stem cell lysates. Sox2 was used as the positive control.

Data information: IP, immunoprecipitation; WB, Western blotting. Source data are available online for this figure.

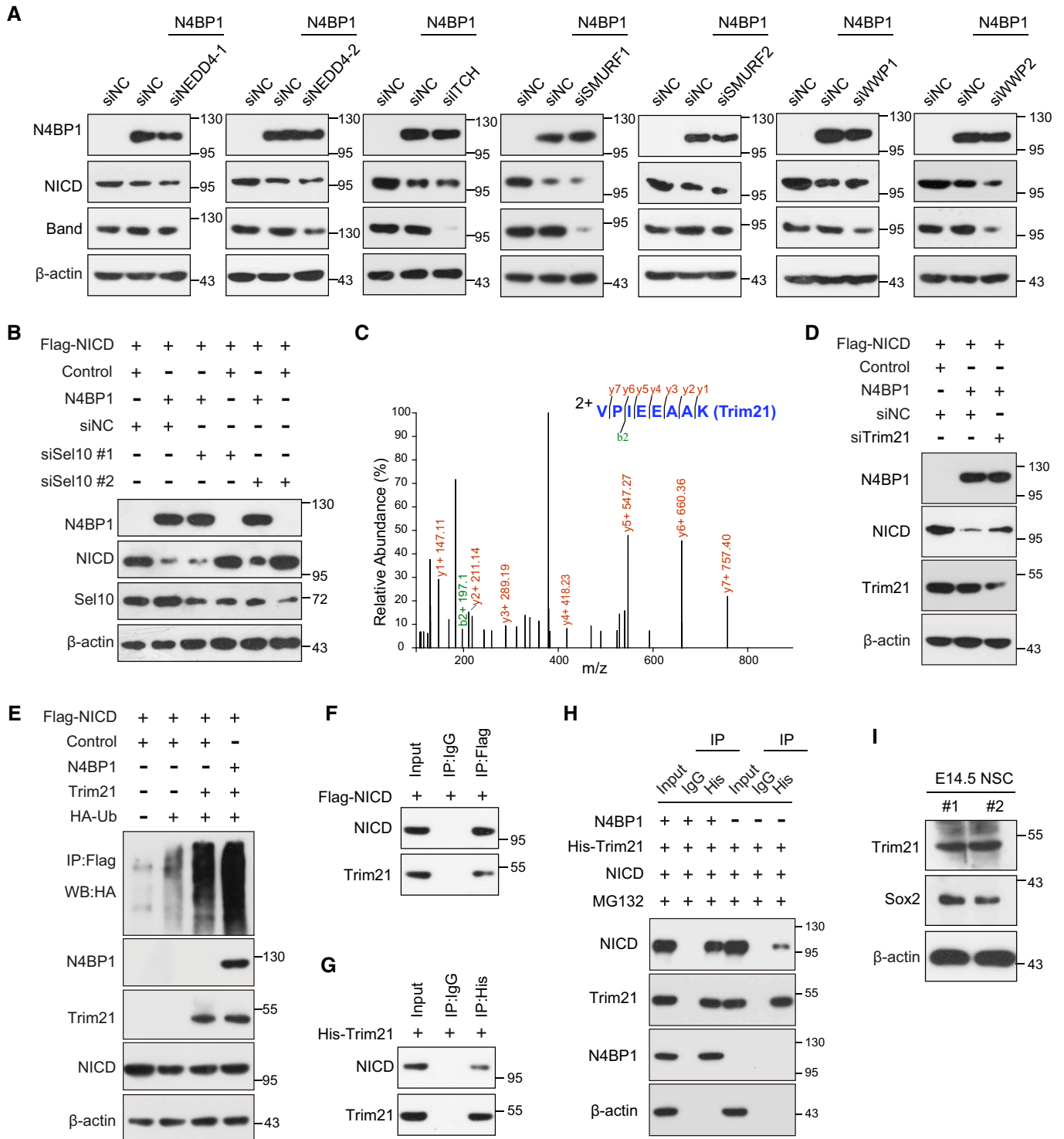


Figure 5.

(Fig EV5D). Intriguingly, we also detected a slight increase of ALDH1L1⁺ astrocytes in N4bp1 cKO mice than that in WT mice (Fig EV5E and F).

To investigate mechanisms of reduction in upper-layer neurons after N4bp1 deletion, we performed terminal deoxynucleotidyl transferase dUTP nick end labeling (TUNEL) staining, and no significant apoptosis was found in E16.5 and P3 cerebral cortex of mice, that excluded enhanced apoptosis in N4bp1-cKO neocortices

(Fig EV5G). Next, we assessed whether the declined generation of upper-layer neurons in N4bp1 cKO mice is due to the change of RGCs fate determination. We used 30 min EdU (single pulse) to label proliferating RGCs at E14.5, the stage to generate upper-layer neurons, and found that the ratio of EdU⁺Sox2⁺ double-labelling cells to Sox2⁺ cells was significantly higher in the N4bp1 cKO mice compared to WT mice (44.14 ± 5.23% versus 54.32 ± 5.9%; Fig 6F

and H). Notably, N4bp1 cKO mice showed a much denser progenitor layer as indicated by EdU labelling and Sox2 staining. Specifically, the EdU-labeled RGCs showed a tendency to be near the lateral ventricular surface when N4bp1 was deleted (Fig 6F). Similarly, proliferating Tbr2⁺ IPCs also displayed an increase but nonsignificant trend in N4bp1-deleted mice compared to WT mice (30.48 ± 10.81% versus 36.79 ± 8.66%; Fig 6G and H). We further used 24-h EdU labelling to analysis the self-renewal versus cell cycle exits of NPCs in WT and N4bp1 cKO mice at E14.5 and E15.5. Immunostaining showed that deletion of N4bp1 led to more EdU⁺ cells staying in VZ and co-labeled with Sox2 (Fig EV5H and I, and Appendix Fig S4A and B), indicating enhanced frequency of self-renewal of RGCs. However, this does not change the fate of the generated neurons at this time. The birthdating experiments showed that the majority of EdU⁺ cells generated at E14.5 are still located in upper layer and co-expressed Cux1⁺, rather than Ctip2 and Tle4⁺ neurons in N4bp1-cKO mice (Appendix Fig S4C). These results suggest that the absence of N4BP1 promotes RGC stemness maintenance and weakens the cell cycle exit of RGC in the mid-later neurogenesis, causing the compromised generation of late-born upper-layer neurons.

To further verify whether N4BP1 deficiency was able to influence NPCs self-renewal *in vitro*, NPCs were isolated from the E14.5 embryo brain of WT and littermate N4BP1 cKO mice, respectively, and cultured as neurospheres. In self-renewal assays, the number and size of neurospheres were determined throughout three serial rounds of passaging. The results showed that the proportion of large NPC neurospheres (diameter > 150 μm) was significantly increased in the N4bp1-cKO group compared to the WT group ($P < 0.01$; Fig 6I and J). Furthermore, the expression of markers characterizing NPCs was detected by western blot. Correspondingly, the deletion of N4bp1 in NPCs led to the obviously increased expression of neural stem markers Nestin and SOX2 (Fig 6K). Notably, the expression of NICD also significantly increased (Fig 6K).

Additionally, the expression of effector genes of Notch signaling pathway, including BLBP, Hes5, and Hey1, was determined by *in situ* hybridization on E16.5 and quantitative PCR on E14.5. BLBP, Hes5, and Hey1 mRNA expression were higher in the E14.5 dorsal telencephalon and E16.5 RGCs in N4bp1 knockout mice than in WT

mice (Figs 6L and EV5J), which further indicates the increased activity of Notch signaling pathway.

Altogether, we determined that N4BP1 negatively regulated the Notch signaling pathway by driving NICD into a ubiquitination-proteolysis process. We also reported that N4BP1 promoted NICD degradation directly through the RAM domain but not the PEST domain. The ubiquitin domain CoCUN was critical for establishing an N4BP1-NICD regulation loop. For the first time, the E3 ubiquitin ligase Trim21 was proven to interact with both NICD and N4BP1, which further enhanced the NICD ubiquitination induced by N4BP1. During neocortical development, N4BP1 was highly expressed in NPCs. Overexpression of N4BP1 in cortical NPCs promoted neural stem cell differentiation, whereas NPCs lacking N4BP1 were sensitized to Notch signaling, resulting in the maintenance of stem-like properties, leading to the production of few cortical neurons (Fig 6M).

Discussion

Notch signaling is a pivotal control mechanism of NPC maintenance and neurogenesis (Yoon & Gaiano, 2005; Kageyama *et al.*, 2009). Active Notch signaling in the embryonic telencephalon promoted RGC identity and blocked neurogenesis (Gaiano *et al.*, 2000; Mizutani & Saito, 2005), while Notch deficiency resulted in severe RGC depletion in the telencephalon (Mase *et al.*, 2021). During the development of the neocortex, Notch signaling has been shown to be highly dynamic and tightly controlled. In the present study, we identified N4BP1 as an antagonist of Notch signaling because it regulated NICD stabilization. Our findings demonstrated that N4BP1 interacted with the E3 ubiquitin ligase Trim21 to mediate NICD degradation and that this effect depended on the RAM domain in NICD. We further found that the ubiquitin-binding activity of the CoCUN domain in N4BP1 was pivotal to mediating NICD ubiquitination. Moreover, we showed that overexpression of N4BP1 promoted NPCs escape from the VZ and SVZ, while the conditional knockout of N4bp1 impaired neurogenesis, which was consistent with the effect of the inhibited or augmented Notch signaling during the development of the neocortex. Our findings reveal a novel mechanism for regulating the Notch signaling pathway.

Figure 6. N4BP1 is necessary for balancing the differentiation and proliferation of RGCs.

- A Comparison of P3 brains of WT (*Emx1^{wt} N4bp1^{wt/wt}*) and conditional N4bp1-knockout (cKO, *Emx1^{Cre} N4bp1^{lox/lox}*) littermate mice; scale bars, 5 mm.
- B Quantification of P3 brain size in control and N4bp1-cKO littermate mice ($n = 9$ for each group).
- C, D Comparison of P3 coronal sections of the dorsal telencephalon in WT and N4bp1-cKO littermate mice. The thickness of the cortical plate was quantified (C). Sections were stained with DAPI and upper-layer marker Cux1(D). The upper images show the dorsal telencephalon neocortex; scale bars, 400 μm. White brackets indicate the thickness of the cortical plate and mark comparable regions of the cortex shown below at higher magnification; scale bars, 100 μm. The pink-dashed boxes are merged images stained with DAPI and Cux1 in the upper layers magnified at 2×.
- E Quantification of cells labeled with various markers ($n = 6$ for Cux1, Brn2, Ctip2, and Tle4 staining) in P3 brain of WT and N4bp1-cKO littermate mice.
- F, G E14.5 dorsal telencephalon of WT and N4bp1-cKO mice were double labeled for EdU (a single pulse on E14.5 for 30 min) and Sox2 (F) or Tbr2 (G). The left column shows the representative merged images at low magnification; scale bars, 200 μm. White-dotted squares mark comparable regions of the cortex shown in EdU⁺ cells, scale bars, 50 μm. White-dotted rectangles mark the EdU⁺ cells in the VZ/SVZ.
- H Quantitative analysis of the fraction of EdU⁺ cells in the E14.5 brains coexpressing Sox2 or Tbr2 ($n = 4$ for each group).
- I, J Representative images and quantification of NPC neurospheres (third passage) derived from N4BP1-cKO and WT littermate mice. Scale bars, 500 μm.
- K Immunoblot of neural stem markers in NPCs from N4BP1-cKO and WT littermate mice.
- L Measurements of Notch target genes (*BLBP*, *Hes5*, and *Hey1*) and *N4bp1* mRNA expression in WT and N4bp1-cKO littermate mice. $n = 3$ for each group.
- M A cartoon showing how N4BP1 regulates NICD to control radial glial cell proliferation or differentiation in the developing mammalian neocortex. N4BP1 interacts with NICD through the RAM domain and the E3 ubiquitin ligase Trim21 to form a tricomplex to ubiquitinate NICD, which targets it for proteolysis via the proteasome.

Data information: The mean ± SD is shown. Statistical analysis was performed by unpaired two-tailed Student's *t* test; * $P < 0.05$; ** $P < 0.01$; and *** $P < 0.001$. Source data are available online for this figure.

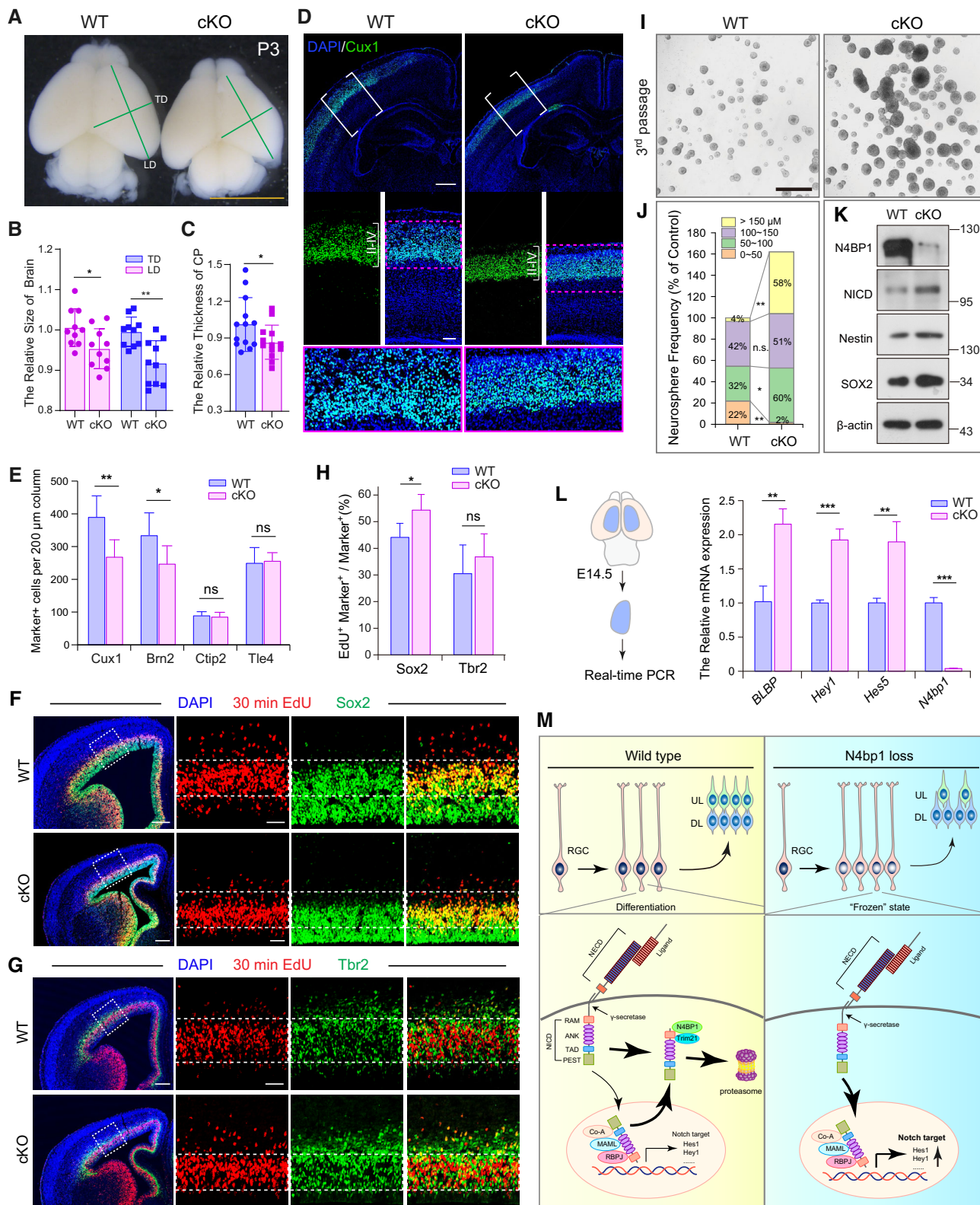


Figure 6.

Understanding the regulatory mechanism of Notch signaling is the basis for clarifying its biological function. Many studies have indicated that the efficient dynamic regulation of NICD is the key control

mechanism of Notch signaling (Mizutani & Saito, 2005; Bray, 2016). As the intensity of Notch signaling is crucial for the fate decisions of neural progenitor cells, Notch signaling can be dynamically self-

terminated or can persist in a context-dependent fashion via the control of NICD dynamics (Kageyama *et al*, 2009; Bray, 2016). After NICD is released from the membrane, the stability and turnover of NICD determine the activity of Notch signaling. In particular, when stem cells differentiate, NICD is eliminated to maintain stemness. This process has been shown to be regulated by the phosphorylation of the PEST domain, which leads to targeted proteasome degradation of NICD after recognition by the E3 ligase FBXW7 (Lee *et al*, 2015). In the present study, we indicated that NICD degradation mediated by N4BP1 depended on the RAM domain, not the PEST domain. Interestingly, Shaye & Greenwald (2002) reported that the RAM domain was necessary and sufficient to mediate the downregulation of LIN-12, the Notch protein in *C. elegans*, and they further found that the 15-amino-acid sequence, named the downregulation-targeting signal (DTS), within the RAM domain, was the key motif in this regulatory effect. In the present study, we demonstrated that RAM was also important for the degradation of mammalian NICD, which has been evolutionarily conserved. Furthermore, for the first time, we identified N4BP1 involvement in this regulatory effect. Notably, although researchers have previously found that NICD degradation was mediated through the lysosomal pathway and depended on the DTS sequence in *C. elegans*, we found that this mechanism has not been conserved. Specifically, the DTS sequence has not been conserved in mammals, and RAM-dependent NICD degradation relies on the ubiquitin-proteasome pathway.

N4BP1 was originally identified as a substrate for the HECT domain-containing ubiquitin ligase Nedd4 (Murillas *et al*, 2002) and has since been found to bind another Nedd4 family E3 ligase, Itch, inhibiting the degradation of Itch-targeted substrates (Oberst *et al*, 2007). Interestingly, although Nedd4 and Itch negatively regulate NICD (Qiu *et al*, 2000; Sakata *et al*, 2004), we found that N4BP1 did not depend on a NEDD4 family E3 ligase; in contrast, it required a Ring family E3 ligase: Trim21 (also named Ro52). The RING domain of Trim21 is both a substrate and catalyst for ubiquitination (Kiss & James, 2022). Following monoubiquitination at the RING domain by the E2 enzyme Ube2W, Trim21 is activated to mediate ubiquitination. The substrates of Trim21 have been reported and include CREB, Snail, Claspin, SET7/9, IRF3/5/7/8, POU2F1, and TXNIP (Kiss & James, 2022). In the present study, we first indicated that NICD is a substrate of Trim21 and found that the interaction was mediated by N4BP1. Trim21 is widely expressed in numerous cell types, including stem cells (Alomari, 2021) and neurons (Kondo *et al*, 2015). TRIM21 increased the ubiquitination and degradation of Oct-1 in cancer stem cells, participating in the self-renewal and maintenance of cancer stem cells (Du *et al*, 2016; Alomari, 2021). Additionally, the tau protein bound by antibodies was the target for destruction by TRIM21, which inhibited tau protein intracellular aggregation and spread between cells, showing clear therapeutic promise for neurodegenerative disease (McEwan *et al*, 2017; Benn *et al*, 2022). In the present study, we showed that Trim21 was highly expressed in the NPCs of embryonic brain tissue, which was consistent with the *in situ* hybridization results of Trim21 reported in the Brain Gene Expression Map database, showing that it was expressed in the neocortex, specifically in the VZ, in the E15.5 mouse brain (Magdaleno *et al*, 2006). Furthermore, we found that Trim21 directly interacted with NICD and N4BP1 and that knocking down Trim21 inhibited the N4BP1-induced degradation of NICD, with overexpression of Trim21 promoting NICD degradation.

Therefore, although it may not be the only ligase involved, Trim21 participates in the cooperative regulation of N4BP1 in the Notch signaling pathway during neural development.

In recent years, N4BP1 has received increasing attention, especially its role in innate immunity. N4BP1 harbors two RNA-binding domains, a KH domain and an RNase NYN domain, which can inhibit HIV-1 replication by interacting with and degrading viral mRNA species (Yamasoba *et al*, 2019). N4BP1 also harbors two ubiquitin-binding domains (UBDs), specifically carrying ubiquitin-associated (UBA)-like domains in the middle region (aa 341–400), and a ubiquitin conjugation to ER degradation (CUE)-like domain, also called a CoCUN domain, in the C-terminus (aa 847–896). Our findings proved that N4BP1 regulated NICD expression at the protein level via multiple lines of evidence: (i) N4BP1 did not downregulate full-length Notch; (ii) KHNYN, an evolutionarily related to N4BP1, carries an RNA-associated domain similar to that in N4BP1 (Santonico, 2020) but cannot degrade NICD; (iii) the results after treating cells with CHX, chloroquine and MG132 differed; (iv) most importantly, when the CoCUN domain is deleted or mutated, N4BP1 did not degrade NICD. To date, N4BP1 has been described based on its ubiquitin-binding features as it can be either polyubiquitinated or monoubiquitinated (Santonico, 2020). N4BP1 lacking a UBA-like or CUE-like domain failed to bind to linear and K63-linked ubiquitin chains (Shi *et al*, 2021). The FP motif in the N4BP1 CoCUN domain recognized the canonical hydrophobic patch in ubiquitin, while mutation of FP abrogated the interaction of N4BP1 and ubiquitin (Neppravishita *et al*, 2019; Santonico, 2020). Our results demonstrated that the CoCUN domain in N4BP1 was crucial to the ubiquitination of NICD in RGCs. Interestingly, N4BP1 has also been reported to bind the deubiquitinating enzyme CEZANNE, resulting in the stabilization of TRAF3 and the degradation of the NF- κ B-inducing kinase NIK in neuroblastoma cells (Spel *et al*, 2018). However, the regulatory mechanism underlying this cellular context-dependent function of N4BP1 needs further exploration.

This study reveals the regulatory effects of N4BP1 on Notch and cortical development. However, several interesting, worthwhile, and open questions need further exploration. Firstly, although our findings showed increased RGC stemness characteristics and reduction of upper-layer neurons in N4BP1-cKO mice, it is worth to investigate more details on how N4BP1 precisely controls RGC stemness, neurogenesis, and gliogenesis. Secondly, although our findings nicely indicated the promotional effect of N4BP1 on neurogenesis, it remains unknown whether N4BP1 can regulate the migration of neurons, as we showed that cells overexpressed N4BP1 were largely restricted to the intermediate zone rather than migrated to the cortical plate. Interestingly, previous studies reported that Notch signaling also seems to perturb neuronal migration in neocortical development. Decreased Notch signaling prevents neurons from transitioning from multipolar to bipolar morphology, resulting in stall migration (Hashimoto-Torii *et al*, 2008). Whether those “frozen” cells are caused by an antagonistic effect to NICD or due to other unknown regulatory roles of N4BP1 remains lack of explanation.

In conclusion, the present study demonstrated, for the first time, that N4BP1 interacts with the E3 ubiquitin ligase Trim21 to mediate NICD ubiquitination and degradation, promoting neurogenesis in the development of the neocortex. Overexpression of N4BP1 in cortical NPCs promotes neural stem cell differentiation, whereas NPCs lacking N4BP1 are sensitized to Notch signaling, resulting in the

maintenance of stem-like properties and leading to the production of few cortical neurons. The interaction between the ubiquitin-binding CoCUN domain of N4BP1 and the RAM domain of NICD is crucial to these effects. Our findings revealed a novel mechanism for regulating the Notch signaling pathway.

Materials and Methods

Mice

N4bp1-fl-neo mice were obtained from the Shanghai Model Organism Center. N4bp1-fl mice were generated by gene targeting in embryonic stem cells, with the N4bp1 gene modified with flox (floxed exon 2), and after embedding the engineered cells in C57BL/6J, chimeric mice were obtained. N4bp1-cKO mice were produced by crossing *Emx1^{cre} N4bp1^{flox/wt}* mice with *Emx1^{cre} N4bp1^{flox/wt}* mice. All mice were given free access to food and water. All animal experiments were conducted according to protocols approved by the Institutional Animal Care and Use Committee at the Academy of Medical Sciences and Peking Union Medical College.

In utero electroporation (IUE)

All pregnant ICR mice were obtained from the Vital River Laboratory Animal Technology Co., Ltd. (Beijing, China) and housed at the Peking Union Medical College Animal Care Facility. IUE was performed as described previously (Shu et al, 2019). All electroporation in this report was performed on E13.5 embryos, and harvested on E16.5 (unless otherwise specified). Expression plasmids were prepared at a final concentration of 3 µg/µl when a single construct was injected unless otherwise specified. For coelectroporation, proper control plasmid was used for diminishing the internal error and adjusting the total amount to 3 µg/µl. The plasmid used for IUE includes pCAG-DN-MAMAL (DN-MAMAL), pCIG-N4BP1 (N4BP1), pCIG-N4BP1 mutant (N4BP1 Mut), pCAG-NICD (NICD), pCAG-NICD-mCherry fusion (NICD-R), pCAG-N4BP1-EGFP fusion (N4BP1-G), pCAG-N4BP1 Mut-EGFP fusion (N4BP1-G Mut), and pCAG-N4BP1 ΔCoCUN-EGFP fusion (N4BP1-G ΔCoCUN). pCAG-IRES-EGFP (pCIG) is used as a control vector for N4BP1 and N4BP1 Mut plasmid, and pCAG-EGFP (pCAG) is the control vector for the other plasmids. The electroporated brains were dissected from the embryos and fixed in 4% paraformaldehyde (PFA) overnight at 4°C. Then, the IUE embryos were dehydrated with 25% sucrose (m/V) at 4°C overnight. The brains were sectioned along a coronal plane at a thickness of 14–16 µm with a cryostat.

In situ hybridization (ISH)

The ISH procedure we followed has been previously described (Zhou et al, 2017). The digoxigenin-labeled probes were synthesized using T7 or SP6 RNA polymerase (New England Biolabs) *in vitro* with the pGEM-3zf plasmid using a DIG RNA labelling kit (Roche Diagnostics) according to the manufacturer's instructions. The labeled slices were imaged using a Nikon microscope (Nikon Instruments Inc.) The sequence of the *N4BP1* probe primer was 5' GCTTGAAGTCTGTGTCT GTGAACCC 3' and 5' CTTTGGATGAGGCAAAGAAGCAAGT 3', respectively.

Immunoprecipitation assays

For immunoprecipitation studies, cells were lysed in RIPA buffer (lysis buffer with 0.5% sodium deoxycholate and 0.1% sodium dodecyl sulfate). Lysates were cleared at 4°C by centrifugation at 12,500 g for 30 min and subsequently incubated with primary antibody overnight at 4°C with rotating. Protein-antibody complexes were incubated with protein A/G-magnetic particles (Roche Diagnostics) for 2 h with rotation. The beads were collected using a magnet stand and washed three times with 1 ml of lysis buffer and then eluted with 0.1 M glycine-HCl (pH = 2.0) for 10 min at room temperature. After elution, an appropriate amount of neutralizing buffer was added to adjust the pH value. One percent of the input and 10% of the immunoprecipitation sample were used for Western blot analysis.

GST pull-down assays

For GST pulldown assays, the sequences of the RAM domain in NICD were inserted into pGEX-6P-1 plasmids to produce GST-tagged fusion proteins. The recombinant vectors were introduced into Transetta cells, which were subsequently induced with IPTG (18°C, 0.2 mM for 12 h). The recombinant GST fusion proteins were purified using Glutathione Sepharose 4B (TaKaRa) beads according to the manufacturer's instructions. Freshly prepared cerebral hemispheres obtained from E14.5 mice were harvested and solubilized in TNTE buffer (50 mM Tris, pH 7.4; 150 mM NaCl; 1 mM EDTA; 10 mM sodium pyrophosphate; 0.5% Triton X-100; 1 mM sodium vanadate; and 25 mM sodium fluoride) containing protease inhibitors (5 µg/ml PMSF, 0.5 µg/ml leupeptin, 0.7 µg/ml pepstatin, and 0.5 µg/ml aprotinin).

The buffer homogenate was centrifuged at 12,500 g for 30 min at 4°C, and the supernatant was incubated overnight at 4°C with glutathione-agarose with rotation. The next day, the beads were precipitated and vigorously washed, and then, the beads were boiled in a sample buffer and analyzed by silver staining or mass spectrometry.

Reporter gene assay

HEK293T or N1E-115 cells were seeded (0.6×10^5) into 24-well (14-mm diameter) plates for 24 h, and then, the cells were transfected with 200 ng of pCBFRE-luc ($4 \times$ CSL) reporter plasmid, 30 ng of pRL-TK plasmid, 100 ng of pCAG-NICD plasmid, and various amounts of an expression plasmid. Then, 24–48 h posttransfection, firefly and Renilla luciferase activities were measured to quantify Notch pathway activity. For endogenous Notch pathway activity measurements, control, DN-MAML or N4BP1 plasmid was transfected into C2C12 cells for 12 h, and then, the transfected cells were cocultured with NIH/3T3 cells for 24 h, and mock cells carried an empty plasmid control. Firefly and Renilla luciferase activities were measured with a Promega dual luciferase assay system. Renilla luciferase activity was used as the internal transfection control. The average values of experiments repeated three times are shown, and each transfection procedure was performed in duplicate for each experiment.

Cell cultures

HEK293T, N1E-115, NIH/3T3 fibroblasts, and C2C12 cells were cultured in Dulbecco's modified Eagle's medium (DMEM) with 10% fetal bovine serum and at 37°C with 5% CO₂ in a humid incubator.

Lipofectamine 3000 (Invitrogen) was used for plasmid transfection according to the manufacturer's instructions. For coculture experiments, transfected C2C12 cells were seeded with approximately the same number of 3T3 cells and incubated for 36 h before analysis.

NPCs were isolated from E14.5 mouse forebrain and digested into single-cell suspension with Accutase (Sigma), and cells were cultured in DMEM/F12 medium supplemented 2% B27 supplement, 20 ng/ml EGF, 20 ng/ml bFGF and 0.2% BSA for proliferation. For self-renewal assays, NPCs from the second passage were dissociated and seeded at very low density (0.5 cell/ μ l) in 24-well plates. After 4 days, neurospheres were quantified, then dissociated and replated at 0.5 cell/ μ l for repeated assays.

Co-transfection

N1E-115 cells or HEK293T cells were co-transfected with a combination of different plasmids. Proper control vector was used for diminishing and eliminating the internal error, and the total amount and ratio of plasmids used for co-transfection were strictly adjusted by mixing them with proper control vectors. pCIG is used as a control vector for pCIG-N4BP1 plasmid, and pCAG is used as a control vector for pCAG-NICD, pCAG-N4BP1-EGFP fusion, pCAG-N4BP1 Mut-EGFP fusion, pCAG-N4BP1 Δ CoCUN-EGFP fusion, pCAG-NICD-mCherry fusion, and pCAG-DN-MAMAL plasmid. For gene knock-down, pLL3.7-shNC is the control for pLL3.7-shN4BP1, and siNC is the negative control for siRNA.

Treatment with cycloheximide

N1E-115 cells were co-transfected with pCAG-NICD or NICD Δ PEST with shNC or shN4BP1-#1 or shN4BP1-#2. HEK293T cells were co-transfected with pCAG-NICD or NICD Δ PEST and the pCIG or pCIG-N4BP1 plasmid. After 48 h of transfection, the cells were treated with 50 μ g/ml cycloheximide (Sigma) for the indicated durations.

Plasmid constructs

The coding sequences for N4BP1 and NICD were subcloned into a pCAG-IRES-EGFP plasmid. The pCIG-N4BP1 and pCAG-NICD plasmids were modified by inserting an EGFP or mCherry sequence to establish an N4BP1-EGFP fusion (N4BP1-G) or NICD-mCherry fusion (NICD-R) construct. The N4BP1 mutant-EGFP fusion plasmid was based on a pCAG-N4BP1 plasmid, with the FP (aa 862–863) motif replaced with a PA motif and with the EGFP sequence inserted. N4BP1 Δ CoCUN-EGFP was modified by inserting the EGFP sequence to establish an Δ CoCUN-EGFP fusion protein. For the luciferase reporter assay experiment, we fused the mouse MAML1 dominant-negative peptide mouse MAML1 (aa 13–74; Maillard et al., 2004) to EGFP by cloning it into a modified pCIG vector.

The pcDNA3.1-flag containing cDNAs for NICD (1,744–2,531), Δ PEST (1,744–2,581), RAM-ANK (1,744–2,126), RAM (1,744–1,872), Δ RAM (1,872–2,531), Δ CoCUN, N4BP1-UP, N4BP1-DOWN, NYN, CoCUN, and KHNYN were generated with routine molecular cloning techniques. The N4BP1 and Trim21 CDSs were cloned into a

pcDNA4.0-myc/his vector. The RAM-ANK (1,704–2,079), RAM (1,704–1,850), Δ RAM (1,851–2,531), ANK (1,851–2,079), and Δ RAM-ANK (2,080–2,531) cDNAs were subcloned into a pEGFP-C2 vector.

For N4BP1-knockdown studies, the sense and antisense oligonucleotides of each shRNA were annealed and cloned into a pLL3.7 vector. An empty vector was used as the negative control (shNC). The targeted shRNA sequences were shN4BP1-#1 5' GGTTCAAA GCAGAACTCAAGT 3' and shN4BP1-#2 5' GAGCAGATTTGAGAAG-CATATTG 3'.

An siRNA-knockdown kit for the NEDD4 family was purchased from RiboBio company. The nonspecific siRNA (siNC) mouse sequences were 5' UUUUCCGAACG UGUCACGUTT 3' and 5' ACGU-GACACGUUCGGAGAATT 3'. The Sel10-#1 specific mouse siRNA sequences were 5' GCAUUUCUCUCUCCAGAGAAGGUTT 3' and 5' ACCUUCUCUGGAGAGAGAAAUGTT 3'. The Sel10-#2 specific mouse siRNA sequences were 5' GGCACUCUAUGUGCUUU-CAUUCTT 3' and 5' GAAUGAAAGCACAUAGAGUGCCTT 3'.

RT-qPCR

Total RNA was isolated with TRIzol reagent, and then the RNA was treated with TURBO DNase (Invitrogen) according to the manufacturer's instructions. Purified total RNA was reverse-transcribed into single-stranded cDNA using SuperScript III Reverse Transcriptase (Invitrogen) in a 20 μ l reaction volume. The reverse transcription product was used for subsequent real-time qPCRs using a SYBR Green system (Takara); GAPDH mRNA was used as the normalization control in all experiments. The results are expressed as fold changes, which were determined using the $\Delta\Delta C_t$ method. The following primers were used:

GAPDH-UP: 5' TTGTCAAGCTCATTTCCTGGTAT 3', and *GAPDH*-DOWN: 5' GTTGGGATAGGCCTCTCTTG 3'[†]; *BLBP*-UP: 5' GCAAA GGGTTTTGTGAATT 3', *BLBP*-DOWN: 5' GTGTGTGATTTTTTA TTTC 3'; *HES5*-UP: 5' TGCAGGAGGCGGTACAGTTC 3', *HES5*-DOWN: 5' GCTGGAAGTGGTAAAGCAGCTT 3'; *HEY1*-UP: 5' GGCA GCCCTAAGCACTCTCA 3', *HEY1*-DOWN: 5' TTCAGACTCCGATCGC TTACG 3'; *N4BP1*-UP: 5' AGTTACTGAGGCTCGATTGGGAGGG 3', and *N4BP1*-DOWN: 5' TGTGGGACAAAACACAGTGATGTTCC 3'.

Western blot

Cells or tissues were lysed with TNTE buffer (50 mM Tris-HCl, 150 mM NaCl, 1 mM EDTA, 0.5% Triton X-100, 25 mM NaF, 1 mM Na₂VO₃) containing protease inhibitors including 1 mM PMSF, 0.6–2 μ g/ml Aprotinin and 1 \times cocktail (CoWin Biotech). Samples with the same amount of total protein in each group were prepared by adding SDS loading buffer into the lysate. Gels were then transferred to nitrocellulose filter membrane. Blots were incubated with related primary antibodies at 4°C overnight after blocking with 5% milk, followed by hybridization with secondary antibodies for 2 h at room temperature. Primary antibodies used in this study: anti-Flag (1:3,000, F7425, Sigma), anti-N4BP1 (1:4,000, ab133610, Abcam), anti-GAPDH (1:5,000, ABS16, Millipore), anti- β -actin (1:5,000, A5441, Sigma), anti-His (1:4,000, AE003, ABclonal Tech), anti-NICD

[†]Correction added on 15 November 2023, after first online publication: The primer sequences *GAPDH*-UP and *GAPDH*-DOWN have been corrected.

(1:3,000, #4147, CST), anti-Notch1 (1:1,000, #4380, CST), anti-HSP90 (1:500, sc-13119, Santa Cruz), anti-N-Cadherin (1:1,000, 610920, BD)[†], anti-HA (1:4,000, ab236632, abcam), anti-Trim21 (1:2,000, A1957, ABclonal Tech), anti-Nestin (1:3,000, A11861, ABclonal Tech), anti-Sox2 (1:4,000, A19118, ABclonal Tech), anti-EGFP (1:500, A-11120, invitrogen), anti-NEDD4-1 (1:2,000, A0552, ABclonal Tech), anti-NEDD4-2 (1:2,000, A9078, ABclonal Tech), anti-ITCH (1:1,000, A8624, ABclonal Tech), anti-SMURF1 (1:2,000, A16559, ABclonal Tech), anti-SMURF2 (1:1,000, A2278, ABclonal Tech), anti-WWP1 (1:2,000, A5269, ABclonal Tech), and anti-WWP2 (1:2,000, A2425, ABclonal Tech).

Tissue preparation and immunofluorescence assay

The embryos or postnatal brains were immersion-fixed in 4% paraformaldehyde overnight at 4°C, cryoprotected in 25% sucrose overnight at 4°C, frozen in O.C.T. compound, and sliced into sections with a cryostat. For immunofluorescence assays, the sections were blocked with 5% normal donkey serum and 0.3% Triton X-100 in phosphate-buffered saline (PBS) for 30 min at room temperature and then incubated with primary antibodies overnight at 4°C. After three brief rinses with PBS, the sections were incubated for 2 h at room temperature in PBS with 0.3% Triton X-100 buffer and fluorophore-conjugated secondary antibodies.

The following primary antibodies were used: rabbit anti-Sox2 (Cat. ab97959, 1:1,000, Abcam), rabbit anti-Tbr2 (Cat. ab23345, 1:500, Abcam), rabbit anti-NeuroD2 (Cat. ab104430, 1:1,000, Abcam), mouse anti-Tle4 (Cat. sc365406, 1:500, Santa Cruz), rat anti-Ctip2 (Cat. ab18465, 1:500, Abcam), rabbit anti-Cux1 (Cat. sc13024, 1:500, Santa Cruz), mouse anti-MAP2 (Cat. ab11267, 1:1,000, Abcam), rabbit anti-Brn2 (Cat. sc-6029, 1:500, Santa Cruz), and rabbit anti-GFAP (Cat. ab7620, 1:5,000, Abcam). The secondary antibodies were donkey anti-rabbit labeled with Alexa Fluor 594, 488, or 647 (Invitrogen). DAPI was used for DNA staining to reveal nuclei, and GFP was visualized without antibody staining. The monoclonal antibody against N4BP1 was produced by ABclonal (amino acids 10–343, ABclonal, Wuhan, China). Confocal images were obtained using an Olympus F1000 confocal microscope with tile scans to visualize the IUE-transfected region or transfected cells. Images were processed using FV10-ASW 3.0 Viewer and Adobe Photoshop. ImageJ software was used to determine mCherry intensity at 594 nm, as shown in Fig 1J. At least three images were analyzed per condition to calculate the mean and standard deviation (SD).

TUNEL staining was conducted on cryosections using in situ Cell Death Detection Kit (11684817910, Roche), following the manufacturer's protocol.

Cell immunofluorescence assays

Cells cultured on coverslips were fixed with 4% fresh paraformaldehyde solution for 20 min at room temperature and then permeabilized with 1% Triton X-100 solution for 20 min at room temperature. The cells were then washed with PBS and incubated with the indicated primary antibodies overnight at 4°C. Next, the cells were incubated with secondary antibodies conjugated to Alexa

594 for 1 h at room temperature. The coverslips were then washed with 0.1% Tween-20 in PBS and mounted using antifade solution with DAPI (Invitrogen).

EdU injection and staining

Pregnant mice were intraperitoneally given a single injection of 5-ethynyl-2-deoxyuridine (EdU) with 75 mg/kg body weight on E14.5 or E15.5, and harvested after 30 min, 24 h, or on P3. EdU staining was performed with cryosections with a Click-iT plus EdU Alexa Fluor Imaging Kit (ThermoFisher) according to the manufacturer's instructions.

Ubiquitination assay

Flag-NICD, pCIG-N4BP1, and HA-Ub were co-transfected into HEK293T cells growing on six-well plates. After 30 h of transfection, MG132 or chloroquine was added to a final concentration of 10 or 20 μ M (Sigma). The cells were solubilized in TNTE, and the protein levels were analyzed by Western blotting. Flag-NICD, pCIG-N4BP1, HA-Ub, and His-Trim21 were co-transfected into HEK293T cells grown in six-well plates. After 12 h of transfection, MG132 was added to a final concentration of 10 μ M. Cells were lysed in lysis buffer. An anti-Flag antibody was used to identify NICD-interacting proteins. Immunoprecipitated proteins were analyzed by Western blotting with an anti-HA antibody.

Nuclear and cytoplasmic fractionation assays and membrane protein extraction

The nuclear and cytosolic fractions were first separated with NE-PER Nuclear and Cytoplasmic Reagents (Thermo Fisher Scientific, 78835) according to the manufacturer's instructions. Briefly, the embryos or N1E-115 cells were washed with cold PBS, Cytoplasmic Extraction Reagent I was added to the cell pellets, the mixture was kept on ice for 10 min, and ice-cold Cytoplasmic Extraction Reagent II was added to the mixture. After centrifuge, the supernatant was transferred to a clean prechilled tube, and the insoluble fraction was suspended in ice-cold Nuclear Extraction Reagent. The pellet suspended in Nuclear Extraction Reagent was vortexed on ice (for 15 s every 10 min for a total of 40 min) and then centrifuged at 16,000 g for 10 min. The supernatant (nuclear extract) fraction was immediately collected.

For membrane protein extraction, HEK293T cells were harvested by centrifugation at 300 g for 5 min after Notch-fl transfection. The membrane protein fractions of cultured cells were obtained with a Mem-PER Plus Membrane Protein Extraction Kit (Thermo Fisher Scientific, 89842), according to the manufacturer's instructions. The nuclear and cytoplasmic fractionations, and membrane proteins were subjected to immunoblotting respectively.

Statistical analysis

The data are presented as the mean \pm SD. They were analyzed using SPSS version 25.0 software for Windows (SPSS Inc., Chicago, IL). Statistical significance between the two groups was determined

[†]Correction added on 15 November 2023, after first online publication: The list of primary antibodies has been updated.

by unpaired two-tailed Student's *t*-test and was determined among multiple groups by one-way ANOVA with *post hoc* Bonferroni tests. A *P* value < 0.05 was considered to be statistically significant. All experiments were independently repeated more than two times with similar results.

For IUE data collection, quantification was performed with coronal sections. The cortex plate was divided into six equal parts to quantify the distribution of GFP⁺ cells, and bin 6 to bin 1 were generated from the inside to the outside. For each comparison, a minimum of three sections from at least two individually electroporated brains were quantified. The hippocampus was used as a guide to find matching positions along two axes (anterior–posterior and medial–lateral) for comparisons between the control and experimental groups.

Data availability

The data from this publication have been deposited to the BioStudies database [www.ebi.ac.uk/biostudies] and assigned the identifier accession number: S-BSST1133.

Expanded View for this article is available [online](#).

Acknowledgements

We thank Professor Weimin Zhong (Yale University) for providing constructive suggestions for the project, Professor Mengsheng Qiu (Hangzhou Normal University) for the ISH technology guidance, and Professor Yan Zhou (Wuhan University) for the gift of different plasmids and N1E-115 cell lines. This work was supported by grants from the National Natural Science Foundation of China (31970772 and 32370883 to P.S.), National Science and Technology Innovation 2030 Grants (2021ZD0200902 to X.P.), and the CAMS Innovation Fund for Medical Sciences (CIFMS; 2021-I2M-1-019 to P.S. and 2021-I2M-1-024 to X.P.)[#].

Author contributions

Zhihua Ma: Data curation; formal analysis; investigation; writing – original draft. **Yi Zeng:** Data curation; formal analysis; investigation; writing – original draft. **Ming Wang:** Data curation; formal analysis; investigation; writing – original draft; writing – review and editing. **Wei Liu:** Formal analysis; investigation. **Jiafeng Zhou:** Formal analysis; investigation. **Chao Wu:** Formal analysis; investigation. **Lin Hou:** Resources; formal analysis. **Bin Yin:** Resources; formal analysis. **Boqin Qiang:** Conceptualization; resources; supervision. **Pengcheng Shu:** Conceptualization; supervision; funding acquisition; methodology; writing – original draft; project administration; writing – review and editing. **Xiaozhong Peng:** Conceptualization; resources; supervision; funding acquisition; writing – review and editing.

Disclosure and competing interests statement

The authors declare that they have no conflict of interest.

References

Aguirre A, Rubio ME, Gallo V (2010) Notch and EGFR pathway interaction regulates neural stem cell number and self-renewal. *Nature* 467: 323–327

- Alomari M (2021) TRIM21 – a potential novel therapeutic target in cancer. *Pharmacol Res* 165: 105443
- Anantharaman V, Aravind L (2006) The NYN domains: novel predicted RNases with a PIN domain-like fold. *RNA Biol* 3: 18–27
- Andersson ER, Sandberg R, Lendahl U (2011) Notch signaling: simplicity in design, versatility in function. *Development* 138: 3593–3612
- Anthony TE, Mason HA, Gridley T, Fishell G, Heintz N (2005) Brain lipid-binding protein is a direct target of Notch signaling in radial glial cells. *Genes Dev* 19: 1028–1033
- Artavanis-Tsakonas S, Delidakis C, Fehon RG (1991) The Notch locus and the cell biology of neuroblast segregation. *Annu Rev Cell Biol* 7: 427–452
- Artavanis-Tsakonas S, Rand MD, Lake RJ (1999) Notch signaling: cell fate control and signal integration in development. *Science* 284: 770–776
- Benn JA, Mukadam AS, McEwan WA (2022) Targeted protein degradation using intracellular antibodies and its application to neurodegenerative disease. *Semin Cell Dev Biol* 126: 138–149
- Borggreve T, Oswald F (2009) The Notch signaling pathway: transcriptional regulation at Notch target genes. *Cell Mol Life Sci* 66: 1631–1646
- Bray SJ (2006) Notch signalling: a simple pathway becomes complex. *Nat Rev Mol Cell Biol* 7: 678–689
- Bray SJ (2016) Notch signalling in context. *Nat Rev Mol Cell Biol* 17: 722–735
- Du L, Li YJ, Fakih M, Wiatrek RL, Duldulao M, Chen Z, Chu P, Garcia-Aguilar J, Chen Y (2016) Role of SUMO activating enzyme in cancer stem cell maintenance and self-renewal. *Nat Commun* 7: 12326
- Dutta D, Sharma V, Mutsuddi M, Mukherjee A (2022) Regulation of Notch signaling by E3 ubiquitin ligases. *FEBS J* 289: 937–954
- Fortini ME (2009) Notch signaling: the core pathway and its posttranslational regulation. *Dev Cell* 16: 633–647
- Fryer CJ, White JB, Jones KA (2004) Mastermind recruits CycC:CDK8 to phosphorylate the Notch ICD and coordinate activation with turnover. *Mol Cell* 16: 509–520
- Gaiano N, Nye JS, Fishell G (2000) Radial glial identity is promoted by Notch1 signaling in the murine forebrain. *Neuron* 26: 395–404
- Gitlin AD, Heger K, Schubert AF, Reja R, Yan D, Pham VC, Suto E, Zhang J, Kwon YC, Freund EC et al (2020) Integration of innate immune signalling by caspase-8 cleavage of N4BP1. *Nature* 587: 275–280
- Gou C, Ni W, Ma P, Zhao F, Wang Z, Sun R, Wu Y, Wu Y, Chen M, Chen H et al (2021) The endoribonuclease N4BP1 prevents psoriasis by controlling both keratinocytes proliferation and neutrophil infiltration. *Cell Death Dis* 12: 488
- Guarani V, Deflorian G, Franco CA, Kruger M, Phng LK, Bentley K, Toussaint L, Dequiedt F, Mostoslavsky R, Schmidt MH et al (2011) Acetylation-dependent regulation of endothelial Notch signalling by the SIRT1 deacetylase. *Nature* 473: 234–238
- Hashimoto-Torii K, Torii M, Sarkisian MR, Bartley CM, Shen J, Radtke F, Gridley T, Sestan N, Rakic P (2008) Interaction between Reelin and Notch signaling regulates neuronal migration in the cerebral cortex. *Neuron* 60: 273–284
- Hoecck JD, Jandke A, Blake SM, Nye E, Spencer-Dene B, Brandner S, Behrens A (2010) Fbw7 controls neural stem cell differentiation and progenitor apoptosis via Notch and c-Jun. *Nat Neurosci* 13: 1365–1372
- Kageyama R, Ohtsuka T (1999) The Notch-Hes pathway in mammalian neural development. *Cell Res* 9: 179–188
- Kageyama R, Ohtsuka T, Shimojo H, Imayoshi I (2009) Dynamic regulation of Notch signaling in neural progenitor cells. *Curr Opin Cell Biol* 21: 733–740

[#]Correction added on 15 November 2023, after first online publication: CIFMS numbers have been corrected.

- Kiss L, James LC (2022) The molecular mechanisms that drive intracellular neutralization by the antibody-receptor and RING E3 ligase TRIM21. *Semin Cell Dev Biol* 126: 99–107
- Kondo A, Shahpasand K, Mannix R, Qiu J, Moncaster J, Chen CH, Yao Y, Lin YM, Driver JA, Sun Y et al (2015) Antibody against early driver of neurodegeneration cis P-tau blocks brain injury and tauopathy. *Nature* 523: 431–436
- Lai EC (2002) Protein degradation: four E3s for the notch pathway. *Curr Biol* 12: R74–R78
- Lee HJ, Kim MY, Park HS (2015) Phosphorylation-dependent regulation of Notch1 signaling: the fulcrum of Notch1 signaling. *BMB Rep* 48: 431–437
- Louvi A, Artavanis-Tsakonas S (2006) Notch signalling in vertebrate neural development. *Nat Rev Neurosci* 7: 93–102
- Magdaleno S, Jensen P, Brumwell CL, Seal A, Lehman K, Asbury A, Cheung T, Cornelius T, Batten DM, Eden C et al (2006) BGEM: an in situ hybridization database of gene expression in the embryonic and adult mouse nervous system. *PLoS Biol* 4: e86
- Maillard I, Weng AP, Carpenter AC, Rodriguez CG, Sai H, Xu L, Allman D, Aster JC, Pear WS (2004) Mastermind critically regulates Notch-mediated lymphoid cell fate decisions. *Blood* 104: 1696–1702
- Mase S, Shitamukai A, Wu Q, Morimoto M, Gridley T, Matsuzaki F (2021) Notch1 and Notch2 collaboratively maintain radial glial cells in mouse neurogenesis. *Neurosci Res* 170: 122–132
- Masek J, Andersson ER (2017) The developmental biology of genetic Notch disorders. *Development* 144: 1743–1763
- McEwan WA, Falcon B, Vaysburd M, Clift D, Oblak AL, Ghetti B, Goedert M, James LC (2017) Cytosolic Fc receptor TRIM21 inhibits seeded tau aggregation. *Proc Natl Acad Sci USA* 114: 574–579
- Mizutani K, Saito T (2005) Progenitors resume generating neurons after temporary inhibition of neurogenesis by Notch activation in the mammalian cerebral cortex. *Development* 132: 1295–1304
- Mizutani K, Yoon K, Dang L, Tokunaga A, Gaiano N (2007) Differential Notch signalling distinguishes neural stem cells from intermediate progenitors. *Nature* 449: 351–355
- Murillas R, Simms KS, Hatakeyama S, Weissman AM, Kuehn MR (2002) Identification of developmentally expressed proteins that functionally interact with Nedd4 ubiquitin ligase. *J Biol Chem* 277: 2897–2907
- Nepravishta R, Ferrentino F, Mandaliti W, Mattioni A, Weber J, Polo S, Castagnoli L, Cesareni G, Paci M, Santonico E (2019) CoCUN, a novel ubiquitin binding domain identified in N4BP1. *Biomolecules* 9: 284
- Oberg C, Li J, Pauley A, Wolf E, Gurney M, Lendahl U (2001) The Notch intracellular domain is ubiquitinated and negatively regulated by the mammalian Sel-10 homolog. *J Biol Chem* 276: 35847–35853
- Oberst A, Malatesta M, Aqeilan RI, Rossi M, Salomoni P, Murillas R, Sharma P, Kuehn MR, Oren M, Croce CM et al (2007) The Nedd4-binding partner 1 (N4BP1) protein is an inhibitor of the E3 ligase Itch. *Proc Natl Acad Sci USA* 104: 11280–11285
- Qiu L, Joazeiro C, Fang N, Wang HY, Elly C, Altman Y, Fang D, Hunter T, Liu YC (2000) Recognition and ubiquitination of Notch by Itch, a hect-type E3 ubiquitin ligase. *J Biol Chem* 275: 35734–35737
- Sakata T, Sakaguchi H, Tsuda L, Higashitani A, Aigaki T, Matsuno K, Hayashi S (2004) *Drosophila* Nedd4 regulates endocytosis of notch and suppresses its ligand-independent activation. *Curr Biol* 14: 2228–2236
- Santonico E (2020) Old and new concepts in ubiquitin and NEDD8 recognition. *Biomolecules* 10: 566
- Schroeter EH, Kisslinger JA, Kopan R (1998) Notch-1 signalling requires ligand-induced proteolytic release of intracellular domain. *Nature* 393: 382–386
- Sharma P, Murillas R, Zhang H, Kuehn MR (2010) N4BP1 is a newly identified nucleolar protein that undergoes SUMO-regulated polyubiquitylation and proteasomal turnover at promyelocytic leukemia nuclear bodies. *J Cell Sci* 123: 1227–1234
- Shaye DD, Greenwald I (2002) Endocytosis-mediated downregulation of LIN-12/Notch upon Ras activation in *Caenorhabditis elegans*. *Nature* 420: 686–690
- Shi H, Sun L, Wang Y, Liu A, Zhan X, Li X, Tang M, Anderton P, Hildebrand S, Quan J et al (2021) N4BP1 negatively regulates NF-kappaB by binding and inhibiting NEMO oligomerization. *Nat Commun* 12: 1379
- Shu P, Wu C, Ruan X, Liu W, Hou L, Fu H, Wang M, Liu C, Zeng Y, Chen P et al (2019) Opposing gradients of microRNA expression temporally pattern layer formation in the developing neocortex. *Dev Cell* 49: 764–785
- Spel L, Nieuwenhuis J, Haarsma R, Stichel E, Bleijerveld OB, Altelaar M, Boelens JJ, Brummelkamp TR, Nierkens S, Boes M (2018) Nedd4-binding protein 1 and TNFAIP3-interacting protein 1 control MHC-1 display in neuroblastoma. *Cancer Res* 78: 6621–6631
- Wu G, Lyapina S, Das I, Li J, Gurney M, Pauley A, Chui I, Deshaies RJ, Kitajewski J (2001) SEL-10 is an inhibitor of notch signaling that targets notch for ubiquitin-mediated protein degradation. *Mol Cell Biol* 21: 7403–7415
- Yamasoba D, Sato K, Ichinose T, Imamura T, Koepke L, Joas S, Reith E, Hotter D, Misawa N, Akaki K et al (2019) N4BP1 restricts HIV-1 and its inactivation by MALT1 promotes viral reactivation. *Nat Microbiol* 4: 1532–1544
- Yoon K, Gaiano N (2005) Notch signaling in the mammalian central nervous system: insights from mouse mutants. *Nat Neurosci* 8: 709–715
- Zhou J, Wang R, Zhang J, Zhu L, Liu W, Lu S, Chen P, Li H, Yin B, Yuan J et al (2017) Conserved expression of ultra-conserved noncoding RNA in mammalian nervous system. *Biochim Biophys Acta* 1860: 1159–1168